Pramana – J. Phys. (2022) 96:84
https://doi.org/10.1007/s12043-022-02331-0

Search for a viable nucleus–nucleus potential in heavy-ion nuclear reactions

T NANDI[1,*], D K SWAMI[1], P S DAMODARA GUPTA[2,3], YASH KUMAR[4], S CHAKRABORTY[1] and H C MANJUNATHA[5,*]

[1]Inter University Accelerator Centre, Aruna Asaf Ali Marg, JNU New Campus, New Delhi 110 067, India
[2]Rajah Serfoji Government College affiliated to Bharathidasan University, Thiruchirappalli620 024, India
[3]Department of Physics, Government First Grade College, Kolar563 101, India
[4]Dipartimento di Fisica "Galileo Galilei", Università di Padova, 35131Padova, Italy
[5]Department of Physics, Government College for Women, Kolar563 101, India
*Corresponding authors. E-mail: nanditapan@gmail.com; manjunatha@rediffmail.com

MS received 19 August 2021; revised 18 November 2021; accepted 7 December 2021

Abstract. We have constructed empirical formulae for the fusion and interaction barriers using a large number of experimental values chosen randomly from the literature available till date. The obtained fusion barriers have been compared with different model predictions based on the proximity, Woods–Saxon and double folding potentials along with several empirical formulas, time-dependent Hartree–Fock theories and experimental results. The comparison allows us to find the best model, which is nothing but the present empirical formula only. Most remarkably, the fusion barrier and radius show excellent consonance with the experimental findings for the reactions meant for the synthesis of superheavy elements also. Furthermore, it is seen that substitution of the predicted fusion barrier and radius in classic Wong formula (Wong, *Phys. Rev. Lett.* **31**:766 (1973) for the total fusion cross-sections agrees very well with the experiments. Similarly, current interaction barrier predictions have also been compared well with a few experimental results available and Bass potential model meant for the interaction barrier predictions. Importantly, the present formulae for the fusion as well as interaction barrier will have practical implications in carrying out physics research near the Coulomb barrier energies. Furthermore, the present fusion barrier and radius provide us with a good nucleus–nucleus potential which is useful for numerous theoretical applications.

Keywords. Nucleus–nucleus potential; heavy-ion; nuclear reaction; fusion barrier height; fusion barrier width.

PACS Nos 13.75.Cs; 25.60.Pj

1. Introduction

The basic characteristics of nuclear reactions are usually described by an interaction consisting of a repulsive Coulomb potential and a short-range attractive nuclear potential. The resultant potential can be expressed as a function of the distance between the centres-of-mass of the target and the projectile nuclei. When a projectile ion approaches the target nucleus, it experiences the maximum force at a certain distance where the repulsive and attractive forces cannot balance each other, the repulsive Coulomb force is always higher. The projectile ion needs to overcome the barrier for coming closer to the target nucleus. This barrier is referred to as the fusion barrier (B_{fu}), which is a basic parameter in describing the nuclear fusion reactions and is simply defined as the maximum of the total potential without the centrifugal term. The kinetic energy of the projectile ion must be adequate to surmount this barrier to enter a pocket adjacent to the barrier at shorter distances, where the nuclei undergo the nuclear fusion processes. Furthermore, the fusion barrier height and its width play a crucial role in the tunnelling process during the sub-barrier fusion. The situation is further complicated by the presence of multiple barriers. The fusion barrier is determined by measuring the excitation function of the nuclear fusion experiments [1] and the same is estimated by many theoretical models such as the Bass potential model [2,3], proximity potential model [4], double folding model [5] and semi-empirical models such as Christensen and Winther (CW) model [6], Broglia and Winther (BW) model [7], Aage Winther

Published online: 20 April 2022

(AW) model [8], Denisov potential (DP) model [9], Siwek-Wilczyńska and Wilczyński (SW) model [10], Skyrme energy density function (SEDF) model [11] and Sao Paulo optical potential (SPP) [12].

In contrast, the quasielastic (QEL) processes, involving energy transfer due to single nucleons or clusters such as α-particles which are smaller than the fusion reactions, excite only nuclear levels in either one of the participating nuclei or in both as soon as the two bodies approach within the range of nuclear forces. The position where the resultant of the Coulomb and nuclear forces is still repulsive and additional energy is required to get the two nuclei interacting over their mutual potential barrier is a barrier which is somewhat smaller than the fusion barrier and is known as the interaction barrier ($B_{\rm int}$). This barrier is measured by the excitation function studies of QEL scattering experiment [13]. Obviously, both the barriers are Coulomb barriers, but they are different from each other. One is characterised by the fusion reaction when the two nuclei fuse to form a compound nucleus and the other by the QEL scattering when the two nuclei enter barely into the strong force regime [2,3] keeping their identities almost intact. However, many a time the distinction is overlooked, see, for example [13,14], though the concept was introduced in the seventies [2,3]. It is worth noting here that it is only Bass who has segregated the appearance of the Coulomb barrier in the two different ways mentioned above: one is the Bass interaction model and the other is the Bass fusion model [2,3].

The above discussions show that the fusion barrier concerns the total reaction process, whereas the interaction barrier indicates a bare minimum effect of the reaction process. Hence, the latter is a measure of the reaction threshold. It appears at the low-energy side relative to the fusion barrier because at all incident energies the total reaction cross-section is larger than the cross-section of any specific channel (quasi-elastic channel). For light nuclear systems, these barriers are quite close, but for heavy ones they may significantly differ. For very heavy nuclear combinations, the fusion barrier loses its meaning altogether whereas the interaction barrier maintains its correct physical meaning. This is the fact according to Bass [2,3], but Zagrebaev [15] is against using different names. However, for convenience we continue here with Bass conventions.

Recently, Sharma and Nandi [16] demonstrated the coexistence of the atomic and nuclear phenomena on the elastically scattered projectile ions while approaching the Coulomb barrier. Here the projectile ion X-ray energies were measured as a function of ion beam energies for three systems ^{12}C(^{56}Fe,^{56}Fe), ^{12}C(^{58}Ni,^{58}Ni) and ^{12}C(^{63}Cu,^{63}Cu) and observed unusual resonance-like structures as the beam energy approaches the fusion barrier energy, according to the Bass model [2,3]. However, resonance would have occurred near the interaction barrier as the technique involved only the elastic phenomenon and thus resembling the quasi-elastic (QEL) scattering experiment [13]. It implies that resonance should have appeared adjacent to the interaction barrier. To resolve this anomaly, we planned to examine both the fusion and interaction barriers in a greater detail. Note that the present attempt is not to make a concrete theoretical model to describe various possible steps of a reaction leading to the final products, but to find the best model available till date so that the above anomaly be resolved. Besides the existing models, we have used a large number of experiments found in the literature to construct an empirical formula for estimating the fusion barriers from the fusion excitation function measurements alone and another for the interaction barriers from the QEL scattering experiments only.

In the next step, we compare the empirical model predictions for fusion barrier with various models based on proximity type of potentials such as Bass potential [2,3] and Christensen and Winther (CW) [6] and Woods–Saxon type of potentials such as Broglia and Winther (BW) [7], Aage Winther (AW) [8], Siwek-Wilczyńska and Wilczyński (SW) [10], SEDF [11] models and the Sao Paulo optical potential (SPP) [12]. Further, the present interaction barrier formula has been compared with the Bass interaction model [2,3]. It is seen that this work will be useful in various applications [1], for example, prediction of $B_{\rm fu}$ or V_B for the formation of the superheavy elements [17] and $B_{\rm fu}$ and $B_{\rm int}$ for the significant physics research near the Coulomb barriers [16].

2. Determination of the barrier heights

Mean fusion barrier height may be obtained from the Gaussian fit of the barrier distribution plot, which is defined as the second derivative of the energy-weighted cross-section $\mathrm{d}^2(\sigma E)/\mathrm{d}E^2$ (point difference) vs. beam energy in the centre-of-mass frame [18,19]. In many articles only the excitation function is reported, and we have converted it into a barrier distribution plot to obtain the mean fusion barrier.

Similarly, the interaction barrier can be obtained from either the QEL excitation function studies or a variety of fusion and fission excitation function measurement. The QEL scattering is affected by the sum of elastic, inelastic and transfer processes, which is measured at backward angles of nearly 180°, where the head-on collisions are dominant. The barrier distribution is obtained by taking the first derivative, with respect to the beam energy, of

the QEL cross-section relative to the Rutherford cross-section, that is, $\frac{-\mathrm{d}}{\mathrm{d}E}(\frac{\mathrm{d}\sigma_{\mathrm{QEL}}}{\mathrm{d}\sigma_R})$ [20]. This method has been examined in several intermediate-mass systems [21,22]. One can notice that the QEL barrier distribution behaves similar to the fusion barrier distribution, although the former is less sensitive to the nuclear structure effects. On the other hand, the thresholds of the reactions corresponding to the low Coulomb barriers are determined using various derivatives of fusion and fission excitation function measurement. One of these has used detection of the recoiling nuclei by the helium-jet technique [23]. In fact, the low Coulomb barriers are the interaction barriers [2].

3. General background

Theoretically, the total nucleus–nucleus interaction potential $V_T(r)$ between the projectile and the target nuclei, in general, is written as a function of the distance r between the two nuclei

$$V_T(r) = V_N(r) + \frac{l(l+1)\hbar^2}{2\mu r^2} + V_c(r), \tag{1}$$

where $V_N(r)$ is the model-dependent nuclear potential, the second term is the centrifugal potential so that $\mu = [A_pA_t/(A_p + A_t)]$ is the reduced mass of the projectile mass A_p and the target nuclei mass A_t in MeV/c^2 units and l represents the angular momentum of the two-body system. When we consider the fusion barrier of the system, l is set to zero which means the centrifugal or the second term is zero. The third term is the Coulomb potential which is given by [24]

$$V_c(r) = \frac{Z_1Z_2e^2}{4\pi\epsilon_0}\begin{cases}\dfrac{1}{r} & \text{for } r \geq R_B\\ \dfrac{1}{2R_B}\left[3-\left(\dfrac{R_B}{r}\right)^2\right] & \text{for } r < R_B.\end{cases} \tag{2}$$

Here the fusion barrier radius $R_B = R_c(A_p^{1/3} + A_t^{1/3})$ where R_c depends on the system as discussed below. Putting the first term of eq. (1) from any particular model, one can solve the fusion barrier radius R_B by using the conditions

$$V_T(r = R_B) = B_{\mathrm{fu}}\frac{\mathrm{d}V_T(r)}{\mathrm{d}r}\bigg|_{r=R_B} = 0$$

and

$$\frac{\mathrm{d}^2V_T(r)}{\mathrm{d}r^2}\bigg|_{r=R_B} \leq 0. \tag{3}$$

Also, $V_T(r = R_{\mathrm{int}}) = B_{\mathrm{int}}$, where R_{int} is the interaction barrier radius. Of course, $V_N(r)$ in eq. (1) needs to be replaced by another appropriate potential to obtain the interaction barrier; for example, the Bass potential model [3] uses different potential forms to estimate the fusion and interaction barriers.

4. Present empirical formula

According to the definition for Coulomb potential given earlier and the shape of the nuclear potential discussed below the barrier radius, B_{fu} and B_{int} may be written as a function of Z_p, Z_t, A_p and A_t. Hence, the experimentally obtained B_{fu} from fusion excitation function measurements and B_{int} from QEL measurements can be plotted against the Coulomb interaction parameter

$$z = \frac{Z_pZ_t}{(A_p^{1/3} + A_t^{1/3})},$$

as shown in figures 1a and 1b, respectively. The fusion experiments used for figure 1a and the QEL experiments used for figure 1b are given in tables 1 and 2, respectively. Fusion data are available for $8 \leq z \leq 286$, whereas QEL data are available for $59 \leq z \leq 313$. We can notice that both B_{fu} vs. z and B_{int} vs. z are nonlinear. The whole range of B_{fu} data has been fitted by two non-linear functions of a sixth-degree polynomial to obtain the reduced chi-square nearly equal to one, whereas the full range of B_{int} data is fitted with a single non-linear function.

The polynomial function that fits the B_{fu} vs. z data extremely well is as follows:

$$\begin{aligned}B_{\mathrm{fu}}^{(1)} =& -1.2725 + 0.9106z + 5.6932\times10^{-4}z^2\\ &+ 2.335\times10^{-5}z^3\\ &- 4.4975\times10^{-7}z^4 + 2.7836\times10^{-9}z^5\\ &- 5.2482\times10^{-12}z^6 \quad \text{for } 8 \leq z \leq 128\end{aligned} \tag{4}$$

and

$$\begin{aligned}B_{\mathrm{fu}}^{(2)} =& -34488.7618 + 1100.6666z\\ &- 14.4066z^2 + 9.9275\times10^{-2}z^3\\ &- 3.7959\times10^{-4}z^4 + 7.6357\times10^{-7}z^5\\ &- 6.3136\times10^{-10}z^6 \text{ for } 128 \leq z \leq 286\end{aligned} \tag{5}$$

and the other function that fits the B_{int} vs. z data is given by

$$\begin{aligned}B_{\mathrm{int}} =& \ 0.09295z^{3/2} - 2.1601z + 35.5879z^{1/2}\\ &- 132.8943 \quad \text{for } 59 \leq z \leq 313.\end{aligned} \tag{6}$$

B_{fu} can be predicted using eq. (4) for any system within $8 \leq z \leq 128$ and eq. (5) for any system within $128 \leq z \leq 286$. Such an empirical formula was constructed in the past [25] as follows:

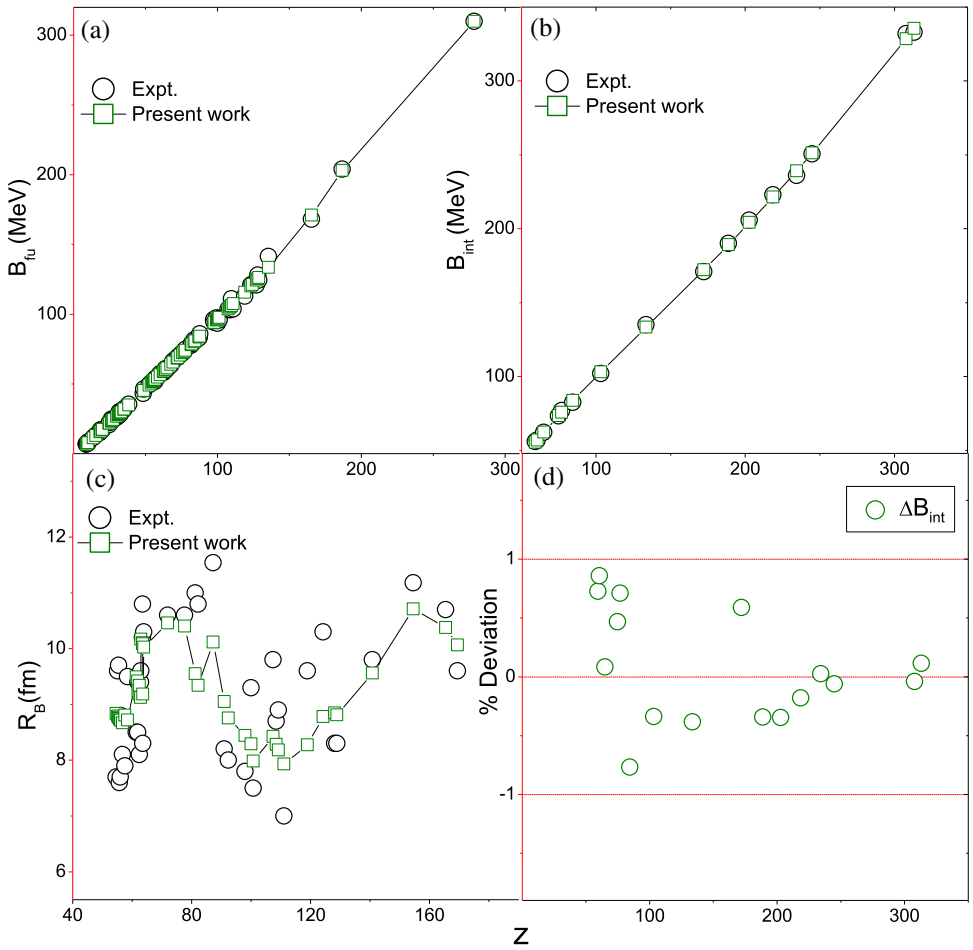

Figure 1. Fusion barrier, interaction barrier, fusion barrier radius and percentage of deviation plots: (**a**) the fusion barrier $B_{\rm fu}$ (MeV), obtained from the fusion excitation function experiments, (**b**) the interaction barrier $B_{\rm int}$ (MeV) from the QEL scattering experiments, (**c**) the fusion barrier radius R_B (fm), (**d**) percentage of deviation of the present value from the experimental $B_{\rm int}$ against the dimensionless parameter z. The percentage of deviation for $B_{\rm fu}$ and R_B are shown in figures 2 and 3.

$$B_{\rm fu} = 0.85247z + 0.001361z^2 - 0.00000223z^3\ \text{MeV}. \tag{7}$$

It was a third degree polynomial function of z, whereas our empirical formula is a sixth degree polynomial function of z.

To obtain R_B, we follow a method involving the reduced fusion barrier position S_B (the separation between the half-density surfaces of the two nuclei) [26]

$$S_B = R_B^{\rm exp} - C_1 - C_2, \tag{8}$$

where the half-density radius of the matter distribution $C_i = (R_i - \frac{b^2}{R_i})$ (for $i = 1, 2$) [27], the sharp radius $R_i = 1.233A_i^{1/3} - 0.98A_i^{-1/3}$ and the measure of the diffuseness of the nuclear surface $b = 0.99$ fm. S_B is fitted with fourth-order polynomial as a function of z as

$$S_B = -46.089 + 2.0478z - 3.0962 \times 10^{-2}z^2 + 1.9278 \times 10^{-4}z^3 - 4.2492 \times 10^{-7}z^4 \tag{9}$$

and R_B is obtained from the reduced fusion barrier position as

$$R_B = S_B + C_1 + C_2. \tag{10}$$

5. Nuclear potential models in literature

In this section, we present different nucleus–nucleus potentials $V_N(r)$, which can be used for obtaining fusion and interaction to compare with the available measured values.

5.1 *Bass potential model*

Bass potential model [2,3] suggests that the Coulomb barrier for the QEL surface reaction is in general different from the Coulomb barrier for fusion. The former results from the QEL processes, where not much mass or

Table 1. The fusion barriers (B_{fu}) for the following two-body systems have been used in figure 1a to obtain the empirical formula for estimating B_{fu} for any system in the bound $8 \leq z \leq 286$ region.

System	z	B_{fu} (MeV)
$^{12}C+^{15}N$	8.83	6.80 [74]
$^{12}C+^{16}O$	9.98	7.50 [75]
$^{12}C+^{26}Mg$	13.71	11.5 [76]
$^{12}C+^{30}Si$	15.57	13.2 [74]
$^{16}O+^{27}Al$	18.84	43.6 [77]
$^{24}Mg+^{26}Mg$	24.63	20.8 [78]
$^{26}Mg+^{32}S$	31.28	27.5 [79]
$^{12}C+^{92}Zr$	35.27	32.3 [80]
$^{16}O+^{72}Ge$	38.32	35.4 [81]
$^{32}S+^{40}Ca$	48.52	43.3 [32]
$^{48}Ca+^{48}Ca$	55.03	51.7 [32]
$^{27}Al+^{70}Ge$	58.42	55.1 [32]
$^{32}S+^{58}Ni$	63.58	59.5 [82]
$^{40}Ar+^{58}Ni$	69.13	66.32 [32]
$^{37}Cl+^{73}Ge$	72.42	69.20 [32]
$^{40}Ca+^{62}Ni$	75.9	72.3 [74]
$^{32}S+^{89}Y$	81.68	77.8 [83]
$^{16}O+^{238}U$	84.43	80.8 [32]
$^{28}Si+^{120}Sn$	87.84	85.9 [32]
$^{48}Ca+^{96}Zr$	97.41	95.9 [84]
$^{40}Ca+^{96}Zr$	100.01	93.6 [82]
$^{40}Ar+^{121}Sb$	109.72	111 [85]
$^{40}Ca+^{124}Sn$	118.95	113 [86]
$^{28}Si+^{198}Pt$	123.18	121 [87]
$^{40}Ar+^{154}Sm$	127.11	121 [88]
$^{40}Ar+^{165}Ho$	135.43	141.4 [32]
$^{40}Ca+^{192}Os$	165.42	168.1 [32]
$^{84}Kr+^{116}Cd$	186.67	204 [89]
$^{74}Ge+^{232}Th$	278.45	310 [89]
$^{86}Kr+^{208}Pb$	285.52	299.00 [9]

energy transfer takes place, whereas maximum mass and energy transfer take place in the latter. Further, the QEL processes become significant as the projectile and the target nuclei approach the range of nuclear force, where the resultant of the Coulomb and nuclear forces is still repulsive. Thus, additional energy is required to get the nuclei within the resultant attractive force, where fusion can occur. According to the Bass interaction model, the barrier responsible in the QEL reactions is called the interaction barrier B_{int} and it can be determined from the elastic scattering experiments [13]. The other barrier is significant in fusion reactions and is defined as the fusion barrier B_{fu}. The latter is equal to the height of the potential barrier for zero angular momentum.

The total effective Bass potential consists of Coulomb, nuclear and centrifugal terms

Table 2. The interaction barriers (B_{int}) for the following two-body systems have been used in figure 1b to obtain the empirical formula for estimating B_{int} for any unknown systems in the range $59 \leq z \leq 313$.

System	z	B_{int} (MeV)
$^{12}C+^{205}Tl$	59.37	56.0 [2,23]
$^{12}C+^{209}Bi$	60.55	57.0 [2,23]
$^{12}C+^{238}U$	65.04	62.2 [2,90]
$^{14}N+^{238}U$	74.82	73.4 [2,90]
$^{16}O+^{205}Tl$	76.99	77.0 [2,23]
$^{16}O+^{238}U$	84.43	82.5 [2,90]
$^{20}Ne+^{238}U$	103.23	102 [2,90]
$^{40}Ar+^{164}Dy$	133.57	135 [2,92]
$^{40}Ar+^{238}U$	172.19	171 [3,92]
$^{48}Ti+^{208}Pb$	188.72	190.1 [13]
$^{54}Cr+^{208}Pb$	202.78	205.8 [13]
$^{56}Fe+^{208}Pb$	218.65	223 [13]
$^{58}Ni+^{208}Pb$	234.38	236 [13]
$^{70}Zn+^{208}Pb$	244.86	250.6 [13]
$^{84}Kr+^{232}Th$	307.86	332 [3,93]
$^{84}Kr+^{238}U$	313.14	33 [3,94]

$$V_l(r) = \frac{Z_p Z_t e^2}{4\pi\epsilon_0 r} + \frac{\hbar^2 l^2}{2\mu r^2} - a_s A_p^{1/3} A_t^{1/3} \frac{d}{R_{pt}} e^{-(\frac{r-R_{pt}}{d})}, \tag{11}$$

where d is the range of nuclear interaction. The influence of fragment (projectile or target nuclei) properties on this potential can be expressed in terms of the dimensionless parameters

$$x = \frac{e^2}{r_0 a_s 4\pi\epsilon_0} \frac{Z_p Z_t}{A_p^{1/3} A_t^{1/3} (A_p^{1/3} + A_t^{1/3})} \tag{12}$$

and

$$y = \frac{\hbar^2}{2m_0 r_0^2 a_s} \frac{A_p + A_t}{A_p^{4/3} A_t^{4/3} (A_p^{1/3} + A_t^{1/3})^2}, \tag{13}$$

where x is the ratio of the Coulomb force to the nuclear force and yl^2 is the ratio of the centrifugal force to the nuclear force at the point of contact, i.e., $r = R_{pt} = r_0(A_p^{1/3} + A_t^{1/3})$ and r_0 =1.07 fm. Here, a_s = 17.23 MeV is the surface constant as used in the liquid drop model of fission, m_0 is the mass of a nucleon and other notations have usual significance. B_{fu} acts at $r = R_{pt} + d_{fu}$ where d_{fu} is the fusion distance. B_{int} is applicable for an interaction distance between the two surfaces (d_{int}) or the centre to centre distance, $R_{int} = R_{pt} + d_{int}$. d_{int} is always longer than d_{fu}, which can be approximately obtained from the relation

$$\frac{d_{fu}}{d} \approx -\frac{\ln x}{(1 - \frac{2d}{R_{pt}})}. \tag{14}$$

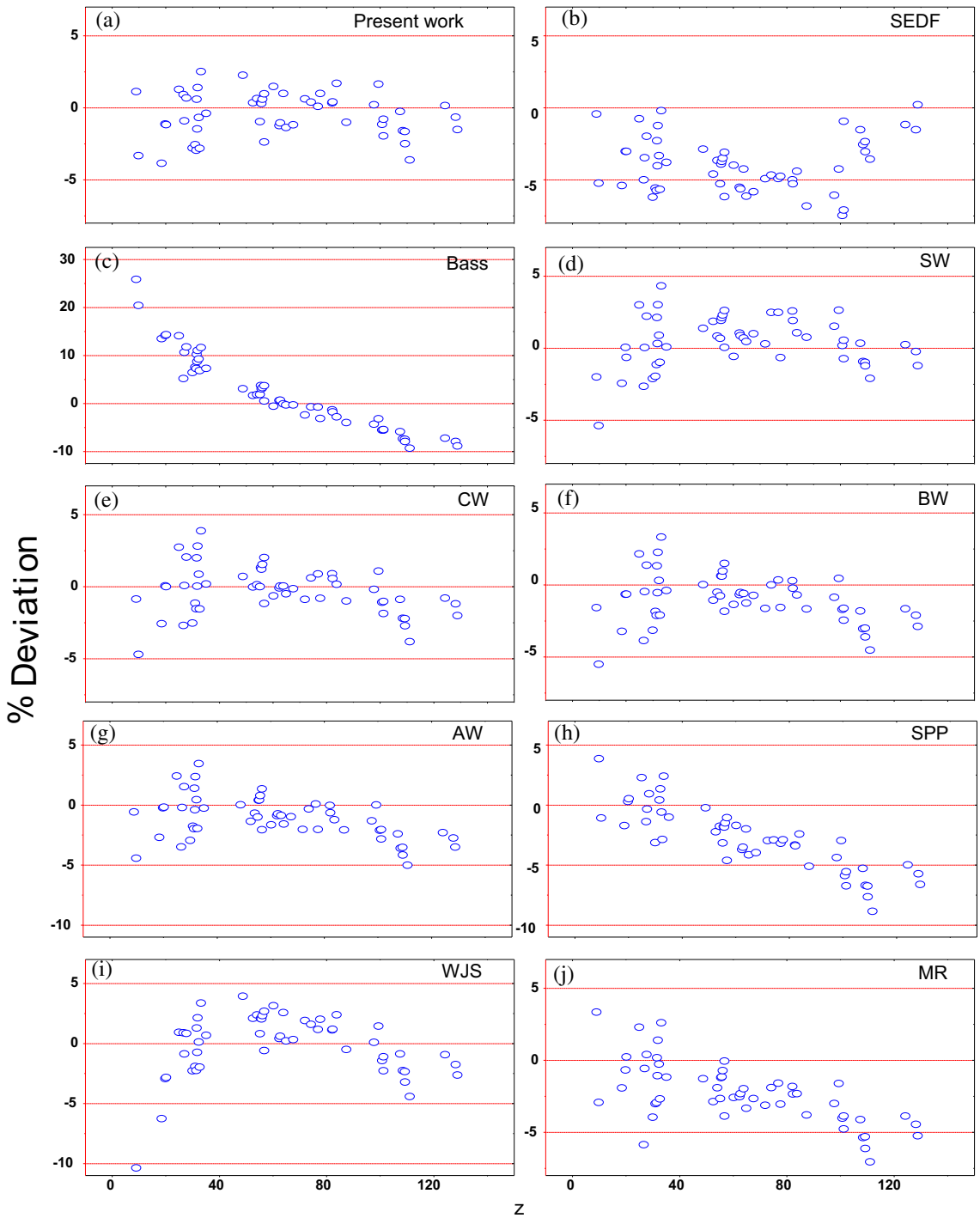

Figure 2. Comparison of the percentage of deviation of different theoretical models and the experimental fusion barriers as a function of z.

$d_{\rm fu}$ varies with the fragments in the nuclear interactions. The barriers $B_{\rm fu}$ and $B_{\rm int}$ can be obtained from

$$B_{\rm fu} = \frac{Z_p Z_t e^2}{4\pi\epsilon_0 R_{pt}} \left\{ \frac{R_{pt}}{R_{pt} + d_{\rm fu}} - \frac{1}{x}\frac{d}{R_{pt}} \mathrm{e}^{\left(-\frac{d_{\rm fu}}{d}\right)} \right\} \tag{15}$$

$$B_{\rm int} = \frac{Z_p Z_t e^2}{R_{pt} + d_{\rm int}} - 2.90 \frac{A_p^{1/3} A_t^{1/3}}{(A_p^{1/3} + A_t^{1/3})} \tag{16}$$

$$d_{\rm int} = 2d = 2 \times 1.35 = 2.70\,\text{fm}. \tag{17}$$

Here, in eq. (17) it is assumed that d is independent of the mass of the nuclei.

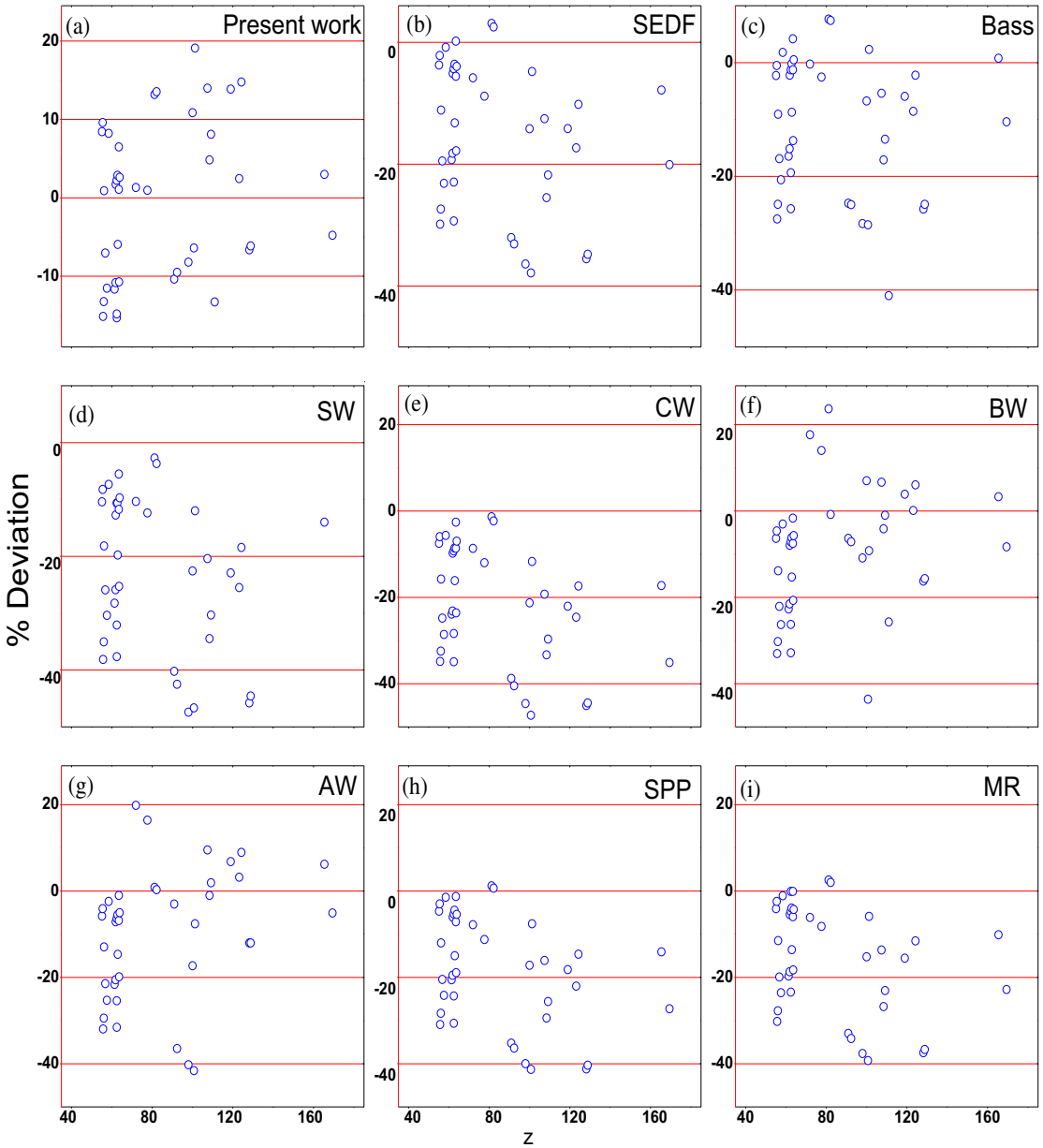

Figure 3. Comparison of the percentage of deviation of different models and the experimental barrier radius as a function of z.

5.2 *Christensen and Winther model*

Christensen and Winther (CW) [6] used elastic scattering trajectory leading to the rainbow pattern that is strongly connected to low-lying target excitation. Hence, the phenomenon happens above the fusion barrier. They derived the nucleus–nucleus interaction potential to represent the nuclear fusion on the basis of semi-classical arguments given by

$$V_N^{\mathrm{CW}}(r) = -50\overline{R}\ \mathrm{e}^{\left(-\frac{r-R_{pt}}{a}\right)}\ \mathrm{MeV}, \tag{18}$$

where

$$R_{pt} = R_p + R_t, \quad \overline{R} = \frac{R_p R_t}{R_p + R_t}$$

and a is the diffuseness parameter ($a = 0.63$ fm). This form is similar to that of the Bass model [2] with different sets of radius parameter.

$$R_i = 1.233A_i^{1/3} - 0.98A_i^{-1/3}\ \mathrm{fm}\ (i = p, t). \tag{19}$$

Here, the radius of the fusion barrier has the form

$$R_B = 1.07(A_p^{1/3} + A_t^{1/3}) + 2.72\ \mathrm{fm} \tag{20}$$

and the total nucleus–nucleus potential for $l = 0$ is

$$U^{\mathrm{CW}}(r) = \frac{Z_p Z_t e^2}{4\pi\epsilon_0 r} + V_N^{\mathrm{CW}}(r) \tag{21}$$

and thus, the fusion barrier can be obtained from $U^{\mathrm{CW}}(r = R_B)$.

5.3 *Broglia and Winther model*

Broglia and Winther (BW) [7] have refined the CW potential [6] to make it compatible with the value of the maximum nuclear force of the proximity potential [4]. This refined force is taken as the standard Woods–Saxon potential given by

$$V_N(r) = \frac{-V_0}{1 + \mathrm{e}^{\frac{r-R_{pt}}{a}}}\,\mathrm{MeV} \tag{22}$$

with

$$V_0 = 16\pi a\gamma \frac{R_p R_t}{R_p + R_t}, \quad a = 0.63\,\mathrm{fm}$$

and

$$R_{pt} = R_p + R_t + 0.29\,\mathrm{fm}. \tag{23}$$

Here the nucleus radius R_i is given by

$$R_i = 1.233A_i^{1/3} - 0.98A_i^{-1/3}\,\mathrm{fm} \quad (i = p, t). \tag{24}$$

The surface energy coefficient (γ) has the form

$$\gamma = \gamma_0\left[1 - k_s\left(\frac{N_p - Z_p}{A_p}\right)\left(\frac{N_t - Z_t}{A_t}\right)\right]\mathrm{eV\,fm^2}, \tag{25}$$

where $\gamma_0 = 0.95\,\mathrm{MeV\,fm^{-2}}$ and $k_s = 1.8$. The total interaction potential of the two heavy ions is

$$U^{\mathrm{BW}}(r) = \frac{Z_p Z_t e^2}{4\pi\epsilon_0 r} + V_N^{\mathrm{BW}}(r) \tag{26}$$

and it displays a maximum, i.e., the fusion barrier and the barrier radius (R_B) is the solution of the following equation:

$$\left.\frac{\mathrm{d}U^{\mathrm{BW}}(r)}{\mathrm{d}r}\right|_{r=R_B} = -\frac{Z_p Z_t e^2}{4\pi\epsilon_0 R_B^2} + \frac{V_0 \mathrm{e}^{\frac{R_B-R_{pt}}{a}}}{a\,(1 + \mathrm{e}^{\frac{R_B-R_{pt}}{a}})^2} = 0 \tag{27}$$

and $U^{\mathrm{BW}}(R_B)$ is the fusion barrier.

5.4 *Aage Winther model*

Aage Winther (AW) [8] slightly adjusted the parameters of the Broglia and Winther potential through an extensive comparison with the experimental data for heavy-ion elastic scattering. The resulting values of a and R_i are as follows:

$$a = \left[\frac{1}{1.17(1 + 0.53(A_p^{-1/3} + A_t^{-1/3}))}\right]\,\mathrm{fm} \tag{28}$$

and

$$R_i = 1.20A_i^{1/3} - 0.09\,\mathrm{fm} \quad (i = p, t) \tag{29}$$

and R_{pt} of the BW model is written as $R_{pt} = R_p + R_t$ only.

5.5 *Siwek-Wilczyńska and Wilczyńki model*

Siwek-Wilczyńska and Wilczyński (SW) [10] have used many reactions to determine an effective nucleus–nucleus potential for reliable prediction of the fusion barriers for the systems that are studied. In this approach, the nucleus–nucleus potential is taken also as the Woods–Saxon shape and is given in eq. (22), where $R_{pt} = R_p + R_t$ and $R_i = R_c A_i^{1/3}$ $(i = p, t)$, the radius parameter R_c is constant, a is the diffuseness parameter and V_0 is the depth of the potential. V_0 is given by

$$V_0 = V_0' + S_{cn}, \tag{30}$$

where S_{cn} is the shell correction energy [28] and

$$\begin{aligned} V_0' &= (M_p + M_t - M_{cn})c^2 + C_{cn} - C_p - C_t \\ &= Q_{\mathrm{fu}} + C_{cn} - C_p - C_t. \end{aligned} \tag{31}$$

Here Q_{fu} is the ground state Q value for fusion and C_i are the intrinsic Coulomb energies [10] as given by

$$C_{cn} - C_p - C_t = C_0, \tag{32}$$

where

$$C_0 = 0.7054\left[\frac{(Z_p + Z_t)^2}{(A_p + A_t)^{1/3}} - \frac{Z_p^2}{A_p^{1/3}} - \frac{Z_t^2}{A_t^{1/3}}\right]\mathrm{MeV}.$$

The Coulomb energy constant is taken from the standard liquid-drop model fit to nuclear masses [29]. Now, eq. (30) can be written as

$$V_0 = Q_{\mathrm{fu}} + C_0 + S_{cn}. \tag{33}$$

For determining the fusion barrier, one considers the nucleus–nucleus potential in the region $R > R_{pt}$ as

$$V(r) = V_N(r) + \frac{Z_p Z_t e^2}{4\pi\epsilon_0 r}. \tag{34}$$

For the region $r < R_p + R_t$, $\mathrm{e}^{[\frac{r-R_{pt}}{a}]} \to 0$, the nucleus–nucleus potential takes the form

$$V(r) = C_0 - V_0 = -Q_{\mathrm{fu}} - S_{cn}. \tag{35}$$

Thus, eq. (34) gives the fusion barrier. It has only two free parameters R_c and a as V_0 is known from eq. (33). These parameters are obtained by fitting the barriers from eq. (34). The experimental $B_{\rm fu}$ values can be obtained where the measured fusion excitation functions are fitted with the following expression:

$$\sigma_{\rm fus} = \pi r_\sigma^2 \frac{\omega}{E\sqrt{2\pi}} \times [X\sqrt{\pi}(1 + \mathrm{erf}(X)) + \exp(-X^2)], \quad (36)$$

where

$$X = \frac{E - B_{\rm fu}}{\sqrt{2}\omega}$$

and erf(X) is the Gaussian error integral of argument X given as

$$\mathrm{erf}(X) = \frac{1}{\sqrt{\pi}} \int_0^X \mathrm{e}^{-t^2} \mathrm{d}t. \quad (37)$$

The fitting gives three parameters: the fusion barrier $B_{\rm fu}$, the relative distance corresponding to the position of the approximate barrier r_σ and the width of the barrier w. However, the values of R_c and a depend on the Coulomb barrier parameter z. For example,

$$R_c = 1.25\,\mathrm{fm} \quad \text{and} \quad a = 0.481\,\mathrm{fm} \quad \text{for } z < 70$$
$$R_c = 1.18\,\mathrm{fm} \quad \text{and} \quad a = 0.675\,\mathrm{fm} \quad \text{for } 70 < z < 130$$
$$R_c = 1.11\,\mathrm{fm} \quad \text{and} \quad a = 0.895\,\mathrm{fm} \quad \text{for } z > 130.$$

5.6 *Skyrme energy density function model*

Skyrme energy density function (SEDF) model has been introduced by Wang *et al* [11,30], where the total binding energy of a nucleus is represented as the integral of the energy density function [31]

$$E = \int H\,\mathrm{d}r. \quad (38)$$

Here energy-density function H has three parts: kinetic energy, Coulomb and nuclear interactions and is generally defined as follows:

$$H(r) = \frac{\hbar^2}{2m}[\tau_p(r) + \tau_n(r)] + H_{\rm coulomb}(r) + H_{\rm nuclear}(r), \quad (39)$$

where τ_p and τ_n are the kinetic energy density for proton and neutron, respectively. The interaction potential $V_B(R)$ is defined as

$$V_B(R) = E_{\rm tot}(R) - E_p - E_t, \quad (40)$$

where $E_{\rm tot}(R)$ is the total energy of the interacting nuclear system, E_p and E_t are the energies of the projectile and the target, respectively, at completely separated distance R. These energies can be calculated by the following relation:

$$E_{\rm tot}(R) = \int H[\rho_{1p}(r) + \rho_{2p}(r - R), \rho_{1n}(r) + \rho_{2n}(r - R)]\mathrm{d}r$$
$$E_p(R) = \int H[\rho_{1p}(r), \rho_{1n}(r)]\mathrm{d}r$$
$$E_t(R) = \int H[\rho_{2p}(r), \rho_{2n}(r)]\mathrm{d}r. \quad (41)$$

The densities of the neutron ρ_n and proton ρ_p for the projectile and the target can be described by the spherically symmetric Fermi function

$$\rho(r) = \frac{\rho_0}{1 + \mathrm{e}^{\frac{(r-c)}{a}}}, \quad (42)$$

where ρ_0, c and a are the parameters of the densities of the participating nuclei in the reactions, which are obtained by using the density-variation approach and minimising the total energy of a single nucleus given by the SEDFM [11,30].

Using the Skyrme energy density formalism, Zanganeh *et al* [32] have constructed a pocket formula for fusion barriers and positions in the range $8 \leq z \leq 168$ with respect to the charge and mass numbers of the interacting nuclei as follows:

$$V_B^{\rm Par} = -0.01[(Z_pZ_t)(A_p^{1/3} + A_t^{1/3})] + 0.20(Z_pZ_t) + 0.60 \quad (43)$$

$$R_B^{\rm Par} = 1.40[A_p^{1/3} + Z_t^{1/3}] - 0.07(Z_pZ_t)^{0.05} + 1.40. \quad (44)$$

We have used eqs (43) and (44) for SEDFM predictions for various reactions as shown in tables 2 and 3. Since the SEDFM is based on the frozen density approximation, the predicted values for each of the considered fusion systems are a bit higher than the corresponding experimental data.

5.7 *Sao Paulo optical potential (SPP)*

This model [12] also takes a Woods–Saxon form for the nuclear potential as given in eq. (22). In the approximation of $\exp((R_B - r)/a) \gg 1$, R_B can be written as

$$R_B = r + 0.65 \ln x, \quad (45)$$

where

$$x = 27.1 \times \frac{A_p^{1/3} + A_t^{1/3}}{Z_pZ_t}$$

Table 3. Comparison of the fusion barrier B_{fu} for different systems with experimental as well as various theoretical models. The reactions are listed in the order of the increasing values of the z parameters. The values for our model is taken from eq. (5).

System	z		SEDF	Bass	SW	CW	BW	AW	SPP	WJS	MR	Pres.
$^{12}C+^{14}N$	8.93	7.00 [74]	7.03	5.19	7.14	7.06	7.11	7.04	6.73	7.72	6.77	7.47
$^{12}C+^{18}O$	9.77	7.45 [95]	7.84	5.93	7.85	7.8	7.86	7.78	7.53	8.46	7.67	7.69
$^{12}C+^{17}O$	9.88	8.20 [32]	7.97	5.97	7.86	7.89	7.94	7.86	7.59	8.54	7.68	7.78
$^{20}Ne+^{20}Ne$	18.42	15.20 [96]	16.02	13.15	15.57	15.59	15.69	15.61	15.46	16.15	15.49	15.78
$^{18}O+^{28}Si$	19.79	16.90 [32]	17.41	14.51	16.89	16.89	17.01	16.94	16.85	17.39	17.01	17.09
$^{16}O+^{28}Si$	20.16	17.23 [32]	17.75	14.76	17.34	17.23	17.34	17.26	17.14	17.71	17.19	17.43
$^{24}Mg+^{24}Mg$	24.96	22.30 [76]	22.47	19.16	21.63	21.69	21.82	21.76	21.79	22.09	21.79	22.01
$^{6}Li+^{144}Sm$	26.35	24.65 [32]	24.65	22.22	24.19	24.32	24.47	24.33	23.78	23.36	24.68	23.35
$^{7}Li+^{159}Tb$	26.6	23.81 [32]	25	22.58	24.44	24.45	24.73	24.64	24.14	23.59	25.21	23.59
$^{16}O+^{40}Ca$	26.94	23.70 [76]	24.52	21.18	23.69	23.68	23.81	23.75	23.78	23.91	23.84	23.91
$^{26}Mg+^{30}Si$	27.68	24.80 [32]	25.29	21.88	24.25	24.29	24.46	24.42	24.57	24.59	24.7	24.62
$^{14}N+^{59}Co$	29.99	26.13 [97]	27.75	24.45	26.68	26.79	26.95	26.9	26.95	26.72	27.16	26.86
$^{26}Mg+^{34}S$	30.96	27.11 [79]	28.62	25.06	27.64	27.42	27.61	27.59	24.07	27.63	27.93	27.81
$^{24}Mg+^{34}S$	31.35	27.38 [79]	28.95	25.39	27.69	27.8	27.96	27.92	24.37	27.99	28.18	28.19
$^{30}Si+^{30}Si$	31.53	28.54 [81]	29.19	25.62	27.93	27.97	28.16	28.14	28.42	28.17	28.49	28.37
$^{24}Mg+^{32}S$	31.69	28.10 [79]	29.23	25.65	28.01	28.09	28.25	28.21	24.61	28.31	28.4	28.51
$^{6}Li+^{208}Pb$	31.77	30.10 [32]	30.27	28.2	30.12	29.97	30.18	30.06	29.4	28.39	30.54	28.59
$^{28}Si+^{30}Si$	31.9	29.13 [78]	29.49	25.91	28.25	28.31	28.47	28.44	28.74	28.51	28.72	28.72
$^{28}Si+^{28}Si$	32.27	28.89 [78]	29.85	26.22	28.63	28.64	28.8	28.76	29.06	28.85	28.97	29.08
$^{20}Ne+^{40}Ca$	32.6	28.60 [32]	30.22	26.64	28.88	29.04	29.2	29.16	29.16	29.42	29.37	29.41
$^{24}Mg+^{35}Cl$	33.14	30.70 [32]	30.76	27.13	29.37	29.51	29.68	29.64	29.66	29.96	29.9	29.92
$^{16}O+^{58}Ni$	35.05	31.67 [32]	32.87	29.36	31.64	31.61	31.79	31.75	31.45	31.99	32.04	31.79
$^{12}C+^{152}Sm$	48.78	46.39 [32]	47.72	44.97	45.75	46.06	46.38	46.38	44.56	46.5	46.98	45.34
$^{18}O+^{124}Sn$	52.58	49.30 [32]	51.57	48.48	48.38	49.31	49.82	49.97	50.4	48.26	50.72	49.12
$^{16}O+^{120}Sn$	53.67	50.41 [98]	52.32	49.3	49.68	50.28	50.73	50.82	51.32	49.25	51.52	50.21
$^{16}O+^{116}Sn$	54.08	50.94 [32]	52.8	50	50.51	50.87	51.2	51.29	51.84	49.72	51.91	50.61
$^{30}Si+^{64}Ni$	55.15	51.20 [99]	53.9	50.25	50.85	51.2	51.59	51.71	52.82	50.78	52.56	51.69
$^{30}Si+^{62}Ni$	55.48	52.20 [99]	54.24	50.56	51.19	51.51	51.87	51.99	53.14	51.11	52.82	52.02
$^{28}Si+^{64}Ni$	55.71	52.40 [99]	54.35	50.82	51.29	51.76	52.08	52.18	53.36	51.32	53	52.24
$^{28}Si+^{62}Ni$	56.04	52.89 [99]	54.74	51.14	51.67	52.07	52.38	52.47	53.68	51.65	53.27	52.57

Table 3. *Continued.*

System	z		SEDF	Bass	SW	CW	BW	AW	SPP	WJS	MR	Pres.
^{40}Ca+^{48}Ca	56.7	52.00 [32]	55.21	51.73	51.97	52.61	52.95	53.07	54.4	52.31	54.01	53.23
^{28}Si+^{58}Ni	56.75	53.80 [99]	55.46	51.82	52.39	52.71	53	53.08	54.37	52.35	53.83	53.28
^{12}C+^{204}Pb	60.17	57.55 [32]	59.84	57.89	57.88	57.92	58.33	58.5	58.53	55.74	59.03	56.71
^{40}Ca+^{48}Ti	62.37	58.17 [100]	61.38	57.82	57.56	58.22	58.56	58.68	60.32	57.92	59.64	58.89
^{35}Cl+^{54}Fe	62.69	58.59 [32]	61.89	58.2	58.08	58.56	58.9	59.02	60.65	58.24	59.95	59.21
^{16}O+^{144}Sm	63.91	61.03 [101]	63.62	61.08	60.6	61	61.39	61.56	62.25	59.45	62.23	60.42
^{37}Cl+^{64}Ni	64.92	60.60 [32]	64.32	60.8	60.32	60.9	61.36	61.56	63.12	60.47	62.62	61.43
^{46}Ti+^{46}Ti	67.54	63.30 [32]	66.99	63.5	62.66	63.39	63.76	63.92	65.81	63.11	64.98	64.05
^{16}O+^{186}W	71.95	68.87 [101]	72.26	70.53	68.66	69.48	69.99	70.27	70.91	67.55	71.02	68.44
^{28}Si+^{92}Zr	74.16	70.93 [80]	74.24	71.43	69.17	70.5	70.93	71.16	72.99	69.81	72.27	70.65
^{40}Ca+^{58}Ni	76.81	73.36 [74]	76.96	73.9	71.54	72.71	73.11	73.3	75.7	72.51	74.52	73.29
^{16}O+^{208}Pb	77.68	74.90 [102]	78.46	77.25	75.39	75.5	76.07	76.42	77.07	7339	77.18	74.15
^{48}Ti+^{58}Ni	82.08	78.80 [103]	82.74	79.86	76.76	78.09	78.57	78.83	81.42	77.91	80.24	78.53
^{36}S+^{90}Zr	82.23	79.00 [104]	83.17	80.39	77.48	78.55	79.18	79.51	81.68	78.11	80.85	78.68
^{19}F+^{197}Au	83.77	81.61 [32]	85.2	83.88	80.73	81.47	82.18	82.61	83.58	79.66	83.5	80.22
^{35}Cl+^{92}Zr	87.34	82.94 [80]	88.6	86.25	82.31	83.76	84.32	84.66	83.35	87.17	86.09	83.77
^{28}Si+^{120}Sn	87.84	85.89 [98]	89.51	86.75	82.82	84.26	84.82	85.16	83.85	87.67	86.59	84.27
^{35}Cl+^{106}Pd	97.7	94.30 [32]	100.02	98.36	92.86	94.48	95.11	95.54	98.43	94.21	97.13	94.11
^{32}S+^{116}Sn	99.36	97.36 [32]	101.5	100.47	94.79	96.31	96.92	97.35	100.24	95.95	98.93	95.75
^{58}Ni+^{60}Ni	100.69	96.00 [32]	103.17	101.33	95.82	97.04	97.63	98.01	101.64	97.36	99.93	97.09
^{40}Ca+^{90}Zr	101.25	96.88 [32]	103.75	102.26	96.34	97.87	98.45	98.86	102.26	97.94	100.63	97.65
^{58}Ni+^{58}Ni	101.27	95.8 [105]	96.7	102.01	96.5	97.59	98.15	98.51	102.25	97.97	100.36	97.67
^{40}Ar+^{122}Sn	107.4	103.6 [106]	105.18	109.7	103.24	104.51	105.47	106.09	109.07	104.51	107.86	103.86
^{40}Ar+^{116}Sn	108.47	103.3 [88]	105.93	110.92	104.26	105.57	106.45	107.02	110.22	105.63	108.84	104.94
^{40}Ar+^{112}Sn	109.22	104.0 [88]	106.44	111.78	105.02	106.3	107.12	107.67	111.02	106.44	109.52	105.71
^{64}Ni+^{74}Ge	109.29	103.2 [88]	106.34	111.37	104.46	106	106.92	107.5	111.09	106.51	109.52	105.77
^{58}Ni+^{74}Ge	111.04	106.8 [107]	107.5	113.49	105.97	107.76	108.49	109.01	112.99	108.39	111.11	107.56
^{34}S+^{168}Er	124.24	121.5 [22]	122.92	130.3	121.2	122.46	123.51	124.3	127.56	122.63	126.11	121.31
^{40}Ar+^{148}Sm	128.14	124.7 [88]	126.6	134.57	124.99	126.19	127.32	128.13	131.85	126.88	130.25	125.45
^{40}Ar+^{144}Sm	128.85	124.4 [88]	127.14	135.41	125.91	126.9	127.98	128.76	132.63	127.66	130.92	126.28

Table 4. Comparison of the fusion barrier radius R_B for different systems with experimental as well as various theoretical models. The reactions are listed in the order of the increasing values of the z parameters. The values for our model is taken from eq. (10). The superscript * indicates that the experimental radii for all the reactions are taken from the ones given in [10] if not mentioned otherwise.

System	z	Expt.*	SEDF	Bass	SW	CW	BW	AW	SPP	MR	Pres.
$^{16}O+^{120}Sn$	53.67	10.73 [98]	1.02	9.88	10.72	10.43	10.32	10.24	10.14	10.07	8.97
$^{30}Si+^{64}Ni$	55.16	9.6	9.96	9.82	10.6	10.32	10.21	10.16	10.05	9.99	8.79
$^{30}Si+^{62}Ni$	55.48	9.7	9.91	9.75	10.5	10.28	10.15	10.1	9.99	9.94	8.77
$^{28}Si+^{64}Ni$	55.71	7.6	9.87	9.69	10.5	10.25	10.11	10.03	9.95	9.9	8.75
$^{28}Si+^{62}Ni$	56.04	7.7	9.81	9.62	10.4	10.2	10.03	9.97	9.88	9.84	8.72
$^{30}Si+^{58}Ni$	56.18	8.8	9.78	9.6	10.4	10.19	10.02	9.94	9.86	9.81	8.72
$^{28}Si+^{58}Ni$	56.75	8.1	9.68	9.47	10.2	10.11	9.89	9.84	9.76	9.71	8.67
$^{40}Ca+^{44}Ca$	57.55	7.9	9.73	9.53	10.3	10.16	9.98	9.9	9.81	9.76	8.81
$^{40}Ca+^{40}Ca$	58.48	9.5	9.58	9.33	10.2	10.04	9.79	9.73	9.64	9.61	8.72
$^{36}S+^{64}Ni$	61.35	8.5	10.14	9.9	10.9	10.53	10.43	10.34	10.25	10.18	9.49
$^{34}S+^{64}Ni$	61.88	8.5	10.05	9.79	10.7	10.47	10.33	10.25	10.16	10.09	9.42
$^{40}Ca+^{50}Ti$	61.94	9.4	9.88	9.61	10.6	10.32	10.15	10.07	9.97	9.91	9.24
$^{40}Ca+^{48}Ti$	62.37	9.4	9.81	9.52	10.4	10.27	10.07	10	9.9	9.84	9.19
$^{32}S+^{64}Ni$	62.44	8.1	9.96	9.67	10.7	10.4	10.23	10.16	10.07	10	9.34
$^{36}Si+^{58}Ni$	62.46	7.7	9.96	9.68	10.6	10.39	10.23	10.13	10.06	10.09	8.84
$^{40}Ca+^{46}Ti$	62.83	9.4	9.74	9.42	10.4	10.21	9.98	9.92	9.82	9.77	9.13
$^{16}O+^{154}Sm$	62.94	9.6	10.87	10.44	11.5	11.15	11.07	11.01	11.04	10.91	10.17
$^{17}O+^{144}Sm$	63.49	10.8	10.78	10.35	11.4	11.08	10.98	10.91	10.94	10.81	10.1
$^{16}O+^{148}Sm$	63.51	10.2	10.77	10.33	11.4	11.08	10.97	10.9	10.93	10.82	10.09
$^{32}S+^{58}Ni$	63.59	8.3	9.78	9.44	10.4	10.26	10.02	9.95	9.87	99.82	9.19
$^{16}O+^{144}Sm$	63.91	10.3	10.71	10.25	11.3	11.02	10.89	10.82	10.86	10.47	10.03
$^{16}O+^{186}W$	71.95	10.6	11.22	10.63	11.7	11.52	8.73	8.5	11.43	11.25	10.46

Table 4. *Continued.*

System	z	Expt.*	SEDF	Bass	SW	CW	BW	AW	SPP	MR	Pres.
$^{16}O+^{208}Pb$	77.68	10.5	11.43	10.77	11.8	11.76	9.03	8.78	11.68	11.47	10.4
$^{36}S+^{96}Zr$	81.21	11	10.66	10.16	11.3	11.15	8.4	10.91	10.87	10.72	9.55
$^{36}S+^{90}Zr$	82.23	10.8	10.53	10	11.2	11.05	10.89	10.77	10.73	10.59	9.34
$^{28}Si+^{120}Sn$	87.84	11.04 [98]	10.68	10.15	11.38	11.24	9.5	9.32	10.95	10.77	9.1
$^{36}S+^{110}Pd$	90.94	8.2	10.83	10.23	11.5	11.38	8.72	8.45	11.09	10.91	9.05
$^{32}S+^{110}Pd$	92.39	8	10.65	10	11.4	11.24	8.57	10.92	10.91	10.7	8.76
$^{64}Ni+^{64}Ni$	98	7.8	10.64	10.01	11.5	11.28	8.65	10.94	10.92	10.74	8.44
$^{40}Ca+^{96}Zr$	100.01	9.3	10.62	9.93	11.4	11.28	8.65	10.91	10.9	10.72	8.29
$^{58}Ni+^{60}Ni$	100.7	7.5	10.34	9.64	11	11.05	10.77	10.62	10.6	10.45	7.98
$^{40}Ca+^{90}Zr$	101.25	10	10.48	9.77	11.2	11.17	10.92	10.76	10.76	10.59	8.09
$^{40}Ar+^{122}Sn$	107.4	9.8	11.03	10.33	11.8	11.69	9.15	8.87	11.38	11.14	8.43
$^{40}Ar+^{116}Sn$	108.47	8.7	10.92	10.19	11.7	11.6	9.06	8.79	11.26	11.03	8.28
$^{40}Ar+^{112}Sn$	109.22	8.9	10.84	10.1	11.6	11.54	8.99	8.73	11.1	10.95	8.18
$^{58}Ni+^{74}Ge$	111.04	7	10.6	9.87	11.4	11.35	8.8	10.93	10.93	10.73	7.93
$^{40}Ca+^{124}Sn$	118.95	9.6	10.96	10.17	11.8	11.72	9.23	8.95	11.35	11.1	8.27
$^{28}Si+^{198}Pt$	123.18	9.8	11.5	10.64	12.3	12.21	9.79	9.49	11.96	11.53	9.56
$^{34}S+^{168}Er$	124.24	10.3	11.35	10.53	12.2	12.09	9.68	9.38	11.81	11.49	8.78
$^{40}Ar+^{148}Sm$	128.14	8.3	11.25	10.44	12.1	12.04	9.65	9.34	11.72	11.41	8.85
$^{40}Ar+^{144}Sm$	128.85	8.3	11.19	10.37	12	11.99	9.6	9.3	11.65	11.35	8.81
$^{40}Ca+^{192}Os$	165.42	10.7	11.54	10.62	12.2	12.55	10.35	10.04	12.21	11.79	10.38
$^{40}Ca+^{194}Pt$	169.4	9.6	11.53	10.6	−−	12.97	10.4	10.09	12.22	11.79	10.06

is a positive dimensionless parameter. Note that the parameter x, which appears in the argument of the logarithm of the above equation, can also be written as $x = \exp((R_B - r)/a)$ and is larger than one in most cases. The barrier potential V_B is given by

$$V_B = \frac{Z_p Z_t e^2}{4\pi\epsilon_0 R_B} - \frac{15}{x+1}. \tag{46}$$

5.8 *Moustabchir–Royer (MR) formula*

Moustabchir and Royer [33] proposed two formulas for the fusion barrier height and radius from a fitting procedure on generalised liquid drop model [34] data on a large number of fusion reactions as follows:

$$V_B = -19.38 + \frac{2.1388 Z_p Z_t + 59.427(A_p^{1/3} + A_t^{1/3}) - 27.07 \ln\left(\frac{Z_p Z_t}{A_p^{1/3}+A_t^{1/3}}\right)}{(A_p^{1/3} + A_t^{1/3})(2.97 - 0.12\ln(Z_p Z_t))} \tag{47}$$

$$R_B = (A_p^{1/3} + A_t^{1/3})\left[1.908 - 0.0857\ln(Z_p Z_t) + \frac{3.94}{Z_p Z_t}\right]. \tag{48}$$

The rms deviations are found to be 0.15 MeV and 0.08 fm in V_B and R_B, respectively.

6. Results and discussions

We have constructed the empirical formulae for the fusion and interaction barriers using the experimental results available in the literature as mentioned already. The fusion barriers $B_{\rm fu}$ can be obtained from eqs (4) and (5), and fusion barrier radius R_B from eq. (10). In table 3, $B_{\rm fu}$ values obtained from various theoretical models for different systems are compared with the experimental results in the rage of $9 \le z \le 129$, which are not used to construct the present fusion barrier formula. Similar comparisons have also been done for R_B in table 4 for the range $55 \le z \le 170$. To check which model gives the best agreement with the experimental results, the differences of both $B_{\rm fu}$ and R_B values between the experiment and a specific model have been plotted as a function of z in figures 2 and 3, respectively. From figure 2, it is seen that the present empirical formula (figure 2a) is within ±4%, most of the SEDF data overestimates up to 7% (figure 2b), Bass model underestimates for $z \le 60$ and overestimates for $z \ge 60$ (figure 2c), SW predicts within ±5% (figure 2d). Similar comparison is found with CW data (figure 2e), BW data (figure 2f) and AW data (figure 2g), while SPP data show an underestimation for z up to 40 and overestimation up to 10% for $z > 40$. On the other hand, figure 3 gives a clear impression that the deviation between the experiment and theory for the fusion barrier radius is much larger than the fusion barrier. Whatsoever, we can find that the present empirical formula (figure 3a) is within ±20%, deviations of the SEDF data are within $^{+40\%}_{-5\%}$ (figure 3b), Bass model estimates within $^{+40\%}_{-6\%}$ (figure 3c) and SW predictions within $^{+50\%}_{-0\%}$ (figure 3d). Similar deviations found with CW (figure 3e), BW data (figure 3f) and AW data show about $^{+40\%}_{-20\%}$ (figure 3g) deviations, while SPP data show an overestimation of 40%. Further, to have a quantitative evaluation on the model predictions, we have obtained the sum of the squared residuals (SSR= $\sum_{i=1}^{n} e_i^2$), where e_i is the ith residual or difference and n is the number of data points. The mean squared errors ($\sigma_\epsilon^2 = {\rm SSR}/(n-2)$) are shown in table 5. The lowest mean squared error on both the fusion barrier and radius is obtained for the present model, thus far the best available formula. Note that the empirical formula of SJW [25] does not predict fusion barrier radius. It is considered to be disqualified in this test. The BW model is the second best and the AW model is the third best in the region considered here.

We can see from figure 1 that very few data exist for $z > 150$, because the reaction mechanism at this region is complex and the data analysis is a tricky affair. If the experimental apparatus is powerful enough in the sense of measuring the number of physical parameters, right kind of data analysis can be possible. Often such apparatus is not available, thereby appropriate analysis method cannot be straightforwardly chosen as discussed below. Therefore, available experimental results are very limited. Whatsoever, the available experimental results for the heavy-ion reactions aiming to form actinide and transactinide elements have been compared with the present formula, WJS formula [25], W D Myers (WDM) model [27] and H C Manjumatha (HCM) formula [26] in table 6. The mean square errors in the present formula, WDM model, WJS formula and HCM formula are found to be 2.26, 4.98, 4.42 and 5.72, respectively. Hence, the predictions from the present formula is the best of all.

The heavy-ion fusion reactions are considered as a dynamic process from the capture of the projectile by the target to the formation of the fully equilibrated compound nucleus [35]. From this, the 'extra push' energy

Table 5. Comparison of mean squared error between the experimental value and a model prediction for the quantities $B_{\rm fu}$ and R_b.

Quantity	SEDF	Bass	SW	CW	BW	AW	SPP	WJS	MR	Present
$B_{\rm fu}$	7.63	15.14	0.82	0.84	1.61	2.41	11.41	3.76	6.88	0.81
R_b	3.05	1.75	5.61	5.21	2.10	2.62	3.92	–	4.42	0.80

Table 6. Comparison of experimental fusion barrier ($B_{\rm fu}$) with the present formula for different reactions in the superheavy region. The last four reactions are used for the reaction contact time experiments [52], where the WJS formula [25] has been used. We show here how much these values differ from the present formula.

System	z	Expt.	Present	WDM [27]	WJS [25]	HCM [26]
^{32}S + ^{232}Th	154.52	155.73 [9]	157.53	153.24	155.99	158.04
^{48}Ca + ^{208}Pb	171.56	173.40±0.1 [39]	173.11	170.19	175.05	176.28
^{50}Ti + ^{208}Pb	187.00	192.60±0.1 [39]	191.82	187.62	192.42	194.04
^{48}Ti + ^{208}Pb	188.71	190.10 [9]	193.02	188.18	194.35	195.10
^{54}Cr + ^{208}Pb	202.79	207.30±0.3 [39]	207.89	203.61	210.22	210.68
^{56}Fe + ^{208}Pb	218.64	223.00 [9]	221.73	220.71	228.14	228.67
^{64}Ni + ^{208}Pb	231.33	236.00 [9]	233.74	233.58	242.43	243.25
^{70}Zn + ^{208}Pb	244.86	250.00 [9]	252.41	248.55	257.61	259.02
^{86}Kr + ^{208}Pb	285.52	299.00 [9]	299.58	292.12	302.44	308.39
^{86}Kr + ^{208}Pb	285.52	303.3 [108]	299.58	292.12	302.44	308.52
^{50}Ti + ^{249}Cf	216.14	–	219.62	218.31	225.32	226.41
^{54}Cr + ^{248}Cm	228.97	–	231.23	232.58	239.78	241.05
^{58}Fe + ^{244}Pu	241.51	–	247.01	245.75	253.85	255.53
^{64}Ni + ^{238}U	252.62	–	266.84	258.22	266.25	268.54

needed to create the compound nucleus was obtained. The values of this energy are in good agreement for the projectile–target combination with $Z_1 \cdot Z_2 \leq 1600$. However, synthesis of the superheavy elements with $Z = 110$–112 and $Z_1 \cdot Z_2 > 1600$ shows a small 'extra push' energy is required [36,37] in contrast to the one predicted by the macroscopic dynamic model [38]. Hence, the capture barriers and fusion barriers are nearly equal for the projectile–target combination with $Z_1 \cdot Z_2 \geq 1600$.

Recently, Banerjee *et al* [39] have precisely measured the capture barriers for the reactions of ^{48}Ca, ^{50}Ti and ^{54}Cr with ^{208}Pb. Since the capture barriers for these reactions are close to the fusion barriers, we can compare these with the fusion barriers and they agree very well with the present formula. Hence, the present formula is an appropriate formula that may be useful for synthesising the superheavy elements also (discussed later). This formula is thus useful for the entire region of $8 \leq z \leq 286$. Of course, for the region $0 < z \leq 8$ where nuclear astrophysics experiments [40] are often conducted, the BW model can be used.

Very recently, Ganiev and Nasirov [41] discussed predictive power of various nucleus–nucleus potentials. The proximity potential [4] and its use in AW model [8] give a deviation of more than 4 MeV from the experimental values of V_B for several fusion reactions. More importantly, the difference increases for the reactions with massive nuclei including the mostly used Bass potential [2,3,18,42] of the proximity potential. For some fusion systems, the results of CW [6] and BW models [43] are close to the experimental data, but these models cannot describe the heavy-ion reactions such as ^{86}Kr+^{208}Pb. In contrast, predictions of a double-folding model (DFM) [41] based on density-dependent Migdal potential [44] are close to all the experimental values including the heavy-ion reactions. We compare the present results for V_B with this DFM model along with the DFM using M3YReid interaction with zero-range exchange part [45] and the Paris CDM3Y3 interaction with finite-range exchange part [46] and experimental data obtained from the cited references in table 7. The mean squared error analysis gives a clear impression that predictions from our formula are the best of all these models.

Synthesis of superheavy elements by heavy-ion reactions is a complex problem because of quasi-fission etc. A fully equilibrated compound system needs to be formed to produce new elements. This depends on entrance channel parameters [47], deformation parameters, orientation, internal excitation, transfer and initial kinetic energy of the projectile [48], which can be picked by the knowledge of theoretical $B_{\rm fu}$. However, the barrier distributions of many heavy-ion reactions used for the synthesis of superheavy nuclei shows double hump behaviour, for example, less mass asymmetric cold fusion reactions. Out of the two humps, the inner peak is the higher peak, while warm fusion reactions, due to higher mass asymmetry, exhibit no double hump barriers [49]. At a given mass asymmetry up to about $\eta = 0.5$ the potential barrier exhibits a two-hump shape, but for larger η it displays only one hump [50]. Hence, double hump problems appear only for the cold fusion type of reactions and the present predictions might represent the higher potential barrier of the corresponding distribution for such reactions. Such scenarios have been discussed later by several researchers from time to time, for example, a very recent article by Royer *et al* [51]. Hence, a precisely known value from this present formula will thus allow us to select the kinetic energy judiciously. Recently, a reaction contact time experiment [52] has made use of the WJS formula [25] (not the WDM model [27], although it is quoted there). We showed just above that uncertainty in the WJS formula [25] is much higher than the present formula. The fusion barriers of the reactions aiming for the superheavy nucleus = 120 have also been compared with different formulae in table 6.

Though the present empirical formula is not specific to a particular form of the nucleus–nucleus potential, the second as well as the third best models are based on the Woods–Saxon potential (eq. (22)) and characterised by the three potential parameters including the potential height parameter V_0, the diffuseness parameter a_0 and the radius parameter r_0. The present formula predicts the fusion barrier and radius pretty well, if we substitute these values in the three equations involved in eq. (3) and solve for these three parameters for a reaction, we can constitute the concerned nucleus–nucleus potential quite well. Such an exercise is followed for several reactions and the Woods–Saxon potential parameters are shown in table 8 and compared with the potential parameters used in the earlier analysis, where mostly the Akyuz Winther parameters [53] have been used, for example [54]. Sometimes the parameters are altered to have an agreement with the fusion cross-section measurements [55]. Even at times, modified Akyuz Winther parameters are chosen by fixing the potential height at 100 MeV [56]. Note that in some models, another parameter is kept fixed, for instance, a_0 is fixed for the BW and AW models as 0.63 fm. In contrast, we have kept all the parameters free while the basic equations are solved (eq. (3)). The values of V_0, a_0 and r_0 span over 26–135 MeV, 0.92–1.76 fm and 0.85–1.24 fm, respectively. In contrast, earlier Akyuz Winther parameters for V_0, a_0 and r_0 fall in the range of 76–105 MeV, 0.67–1.06 fm and 1.06–1.19 fm, respectively.

Once we solve the potential parameters V_0, a_0 and r_0 by the above prescriptions and assume the tail of the

Table 7. Comparison of the fusion barrier heights (second column) ($V_B^{\exp}$) (unit is MeV) with various theoretical results calculated by the DFM V_B^{DFM} (third column), the DFM potential using the M3YReid interaction with zero-range exchange part ($V_B^{\delta R}$) (fourth column) and using the Paris CDM3Y3 interaction with finite-range exchange part (V_B^{Pf}) (fifth column), respectively. All these DFM values have been taken from table 3 of [41]. In the last column and last row, we give the present values ($V_B^{\mathrm{Pres.}}$) and mean squared error of each set of theoretical values, respectively.

Proj.+Targ.	z	$V_B^{\mathrm{exp.}}$	V_B^{DFM}	$V_B^{R\delta}$	V_B^{Pf}	$V_B^{\mathrm{Pres.}}$
^{16}O+^{92}Zr [109]	45.49	42.00	43.50	42.26	41.14	42.08
^{12}C+^{204}Pb [110]	60.17	57.60	57.90	58.61	57.30	56.70
^{16}O+^{148}Sm [101]	63.51	59.80	61.10	61.19	59.61	60.03
^{17}O+^{144}Sm [101]	63.49	60.60	60.80	61.10	59.53	60.00
^{16}O+^{144}Sm [101]	63.91	61.00	61.40	61.53	59.94	60.42
^{28}Si+^{92}Zr [110]	74.16	70.90	71.80	71.46	69.59	70.65
^{16}O+^{208}Pb [102]	77.68	74.55	75.30	77.08	75.40	74.15
^{36}S+^{96}Zr [104]	81.21	76.70	77.80	77.65	75.45	77.67
^{34}S+^{89}Y [83]	80.99	76.90	78.50	77.55	75.42	77.45
^{32}S+^{89}Y [83]	81.68	77.80	79.50	78.21	76.04	78.14
^{36}S+^{90}Zr [104]	82.23	78.00	79.10	78.26	76.01	78.68
^{19}F+^{197}Au [101]	83.77	80.80	81.10	83.83	81.90	80.22
^{35}Cl+^{92}Zr [110]	87.34	82.90	84.50	83.57	81.15	83.77
^{19}F+^{208}Pb [111]	85.88	83.00	83.50	85.26	83.25	82.31
^{40}Ca+^{96}Zr [105]	100.01	94.60	96.50	97.01	94.32	96.41
^{40}Ca+^{90}Zr [105]	101.25	96.90	98.10	97.78	95.01	97.65
^{28}Si+^{144}Sm [112]	104.86	104.00	102.20	104.37	101.72	101.28
^{40}Ca+^{124}Sn [86]	118.95	113.10	114.90	117.89	114.96	115.73
^{28}Si+^{208}Pb [91]	128.10	128.10	126.10	130.90	128.08	126.34
Mean squared error			1.88	3.77	1.94	1.56

Table 8. Comparison of the Woods–Saxon potential parameters V_0 (MeV), r_0 (fm), a_0 (fm) and $\hbar\omega$ from the present empirical formula and other models. The value marked with the superscript (*) indicates that Akyuz Winther (AkW) parameters [53] are altered to have agreement with the measurements. Modified Akyuz Winther (MAkW) parameters are obtained by fixing $V_0 = 100$ MeV and then calculating the values of a_0 and r_0 from the AkW model. The width $\hbar\omega$ is obtained from eq. (48).

Systems	Present work				Other models					Ref.
	V_0	a_0	r_0	$\hbar\omega$	V_0	a_0	r_0	$\hbar\omega$	Model	
^{19}F+^{181}Ta	45.30	1.17	1.15	3.79	104.5	0.700	1.120	5.21	AkW*	[55]
^{16}O+^{154}Sm	26.40	0.92	1.24	4.19	100.0	1.060	1.019	3.85	MAkW	[56]
^{19}F+^{208}Pb	67.73	1.45	1.06	3.51	100.0	1.060	1.059	4.34	MAkW	[56]
^{64}Ni+^{64}Ni	135.07	1.76	0.85	2.61	75.98	0.676	1.190	5.06	AkW	[54]
^{36}S+^{90}Zr	53.72	1.18	1.12	3.27	100.0	0.970	1.070	3.74	MAkW	[56]

nuclear potential to be exponential with diffuseness a_0, one can readily obtain R_B from [57]

$$V_0 = \frac{Z_1 Z_2 e^2}{R_B}\left(1 - \frac{a_0}{R_B}\right). \tag{49}$$

We can obtain now another important parameter called the barrier width ($\hbar\omega$) from the relation given by Rowley *et al* [19] as follows:

$$(\hbar\omega)^2 = \frac{\hbar^2 V''(R_B)}{\mu} = \frac{Z_1 Z_2 e^2 \hbar^2}{\mu R_B^2}\left(\frac{1}{a_0} - \frac{2}{R_B}\right). \tag{50}$$

Use of these barrier radius and width in the Wong's phenomenological formula [58] gives us the fusion cross-section as follows:

$$\sigma_{\rm fu}^{\rm Wong} = \frac{\hbar\omega R_b^2}{2E} \ln\left[1 + \exp\frac{2\pi(E - V_B)}{\hbar\omega}\right]. \tag{51}$$

We made an attempt to check whether the predicted fusion barrier and radius from the present formula can reproduce the measured excitation fusion, i.e., fusion cross-section as a function of the centre of mass energy of the projectile. It is done by a direct substitution of R_B and $\hbar\omega$ in the classic Wong formula [58] given above for many reactions. For example, figure 4 shows a comparison for four reactions: ^{19}F+^{181}Ta [55], ^{16}O+^{208}Pb, ^{16}O+^{154}Sm and ^{58}Ni+^{54}Fe [56]. The comparison of the total fusion cross-section between the phenomenological formula [58] and experiment displays a very good agreement for $E_{\rm cm} > B_{\rm fu}$ and a departure starts appearing at low energies, $E_{\rm cm} < B_{\rm fu}$, except for the reaction ^{16}O+^{154}Sm, because of the strong channel coupling effects for some reactions in the sub-barrier region [59]. The present scenario reiterates the fact that no single, energy-independent potential can simulate the fusion cross-sections at the sub-barrier region, where the well-known influence of the coupling effects is vital. A recent study [60] has discussed the sub-barrier fusion properties on a different view point, which shows the importance of the projectile mass and surface energy coefficients in heavy-ion fusion at sub-barrier energies. Further, it finds the essence of the fusion Q-value rule [61] for some fusion systems.

It is worth mentioning that owing to deformation in the projectile and/or target nuclei, a distribution of barrier heights is observed in the experiments. The fusion barrier height from the present empirical formula represents an average value in the case of such distributions. Obviously, the barrier width also shows an average value and its value for certain reactions are compared with other models in table 8.

In recent years, microscopic mechanisms which can impact the nucleus–nucleus potential has been studied in the framework of time-dependent Hartree–Fock

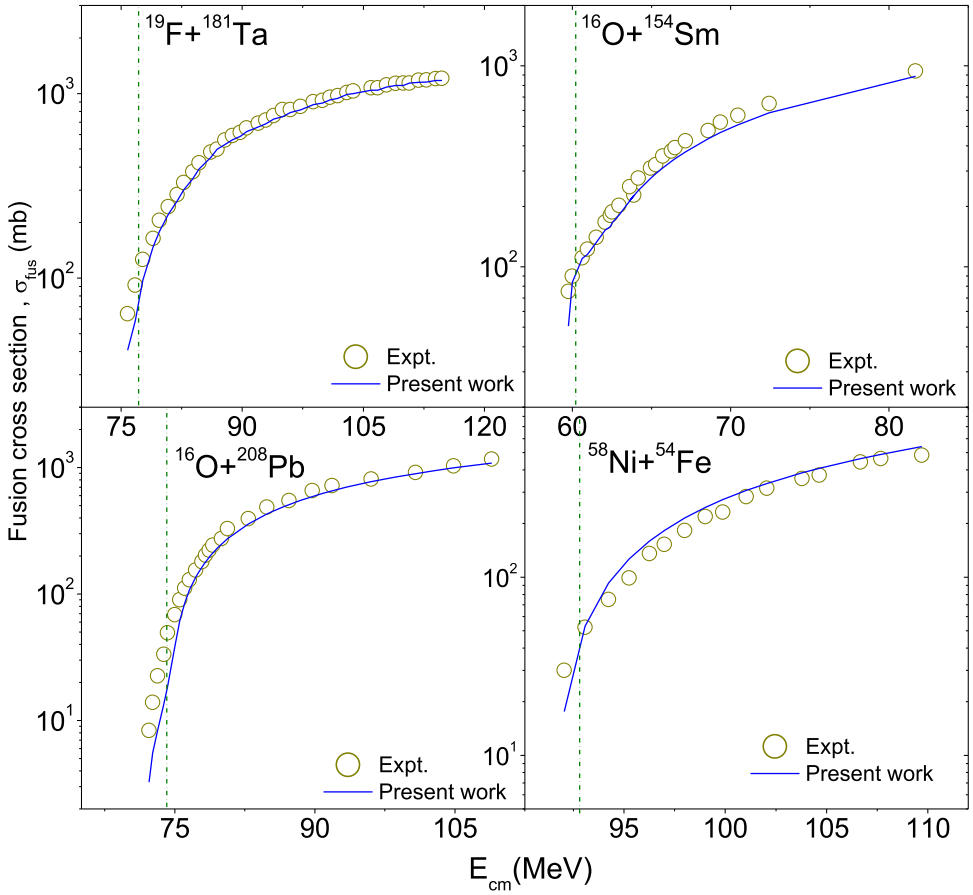

Figure 4. Comparison of total fusion cross-section between the theory and the experiment as a function of $E_{\rm cm}$ for the reactions (**a**) ^{19}F+^{181}Ta [55], (**b**) ^{16}O+^{154}Sm [56], (**c**) ^{16}O+^{208}Pb [102] and (**d**) ^{58}Ni +^{54} Fe. The dashed vertical line indicates the fusion barrier for the corresponding reaction.

(TDHF) approach [62] to provide a rather unique tool for describing nuclear structure and nuclear reactions over the whole nuclear chart. Assuming that the densities of the target and projectile remain constant and equal to their respective ground-state densities, this leads to the so-called frozen density TDHF (FD-TDHF) approximation. Washiyama and Lacroix [63] considered a different approach based on a macroscopic reduction of the mean-field dynamics, called dissipative dynamics in TDHF (DD-TDHF). We have compared the DD-TDHF predictions for the fusion barrier and barrier radius for several reactions with our predictions and available experimental values in table 9, and noticed a good agreement. In recent years, Simenel and his co-workers [64,65] and Yilmaz *et al* [66] have applied TDHF without any approximation to verify the FD-TDHF and DD-TDHF predictions in several cases and found good accordance. Mean squared error is given in the bottom row of the table, which implies that the DD-TDHF predictions with low $E_{\rm cm}$ are the best if we judge both V_B and R_B simultaneously.

Let us briefly discuss the data analysis issue of the heavy-ion reactions here. When a projectile collides with a target nucleus near the fusion barrier energy, besides the evaporation residues (ER) and binary fission [67], the quasi-fission [38,68] is another process that contributes considerably in the reaction cross-sections. Furthermore, quasi-fission occurs before the target and projectile fuse into a compound nucleus not only for the heavy systems $z_t \cdot z_p > 1600$ but also in much lighter systems $z_t \cdot z_p \approx 800$ [69], which results in the hindrance of the formation of ER from the equilibrated compound nucleus. The fusion–fission can also take place from an incomplete fusion reaction [70,71], in which only a part of the projectile fuses with the target and the incompletely fused binary system equilibrates in the compound nucleus. Often, the quasi-fission products are considered as the products of deep inelastic collisions [72] in the experimental data analysis and their contribution is obviously not included in the capture cross-section, and the estimation of the fusion probability from such analyses appears unreliable. If the effect

Table 9. Comparison of the present fusion barrier $B_{\rm fus}^{\rm Pres.} = V_B^{\rm Pres.}$ energy (in MeV) and radii (in fm) of the Coulomb barrier extracted from the DD-TDHF method [63]. $V_B^{\rm DD}$ (high $E_{\rm cm}$) refers to the barrier deduced for $E_{\rm cm} > V_B^{\rm FD}$, while $V_B^{\rm DD}$ (low $E_{\rm cm}$) corresponds to the lowest Coulomb barrier deduced from TDHF using $E_{\rm cm} < V_B^{\rm FD}$ and available experimental values. The reactions are listed in the order of the increasing values of z parameters. Mean squared errors (MSE) are given at the bottom row. See text for details.

Reaction	$V_B^{\rm FD}$	$V_B^{\rm DD}$ (high $E_{\rm cm}$)	$V_B^{\rm DD}$ (low $E_{\rm cm}$)	$V_B^{\rm Pres.}$	$V_B^{\rm exp}$	$R_B^{\rm FD}$	$R_B^{\rm DD}$ (high $E_{\rm cm}$)	$R_B^{\rm DD}$ (low $E_{\rm cm}$)	$R_B^{\rm Pres.}$	$R_B^{\rm exp}$
^{16}O + ^{16}O	10.2	10.13	10.12	10.41	10.61 [74]	8.4	8.46	8.52		7.91 [74]
^{16}O + ^{40}Ca	23.5	23.36	23.07	23.91	23.06 [74]	9.2	9.18	9.50		9.21 [74]
^{16}O + ^{48}Ca	23.0	22.77	22.48	23.01		9.4	9.50	9.75		
^{40}Ca + ^{40}Ca	54.7	54.54	53.35	55.00	52.80 [113]	9.8	9.82	10.32	8.72	
^{40}Ca + ^{48}Ca	53.4	53.24	52.13	53.53	52.00 [114]	10.1	10.09	10.56	8.88	9.99 [114]
^{48}Ca + ^{48}Ca	52.4	52.13	50.97	51.56	51.49 [114]	10.3	10.38	10.82	9.02	10.16 [114]
^{16}O + ^{208}Pb	76.0	75.91	74.51	74.15	74.52 [114]	11.8	11.74	12.14	10.41	11.31 [114]
^{48}Ca + ^{90}Zr	99.8	99.98	97.71	97.65	96.88 [114]	10.8	10.63	11.27	8.55	10.53 [114]
MSE	3.51	3.37	0.34	1.74	–	0.17	0.13	0.99	3.63	–

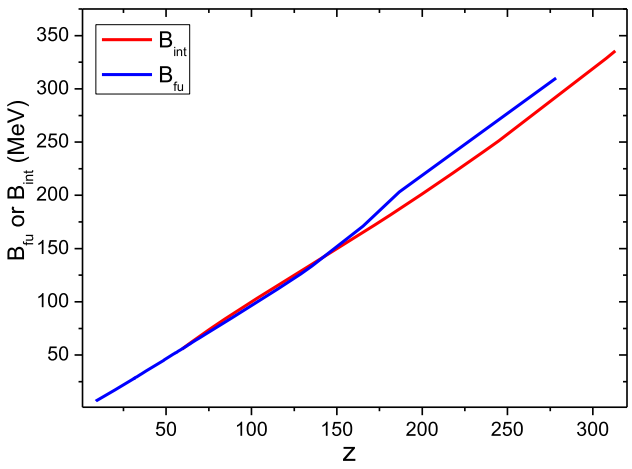

Figure 5. Comparison of interaction barrier ($B_{\rm int}$ with fusion barrier $B_{\rm fus}$) as a function of Coulomb interaction parameter.

of quasi-fission and incomplete fusion–fission reaction are not considered in the analysis, the reaction cross-sections will certainly be erroneous. Such circumstances may of course distort the value of the fusion barrier if the contribution of the quasi-fission and incomplete fusion–fission reaction vary with the beam energy. However, a recent thorough study shows that the cross-section measured from the fission products $\sigma_{\rm fis}$ could be well reproduced by scaling the capture cross-section $\sigma_{\rm cap}$ for a cold fusion by constant factors of 0.75 for ^{48}Ca, 0.48 for ^{50}Ti and 0.22 for ^{54}Cr projectiles on ^{208}Pb target [39]. Hence, the present empirical formula is suitable for realistically predicting the fusion barrier for any new reactions planned in search of the formation of the super-heavy elements.

Let us now discuss the interaction barriers, which can be obtained from eq. (6) and compared with the experiments and model predictions. The experimental values available have been compared with the present empirical formula in table 10. These experimental values compare far better with the present formula than with the Bass model. Mean squared error turns out to be 3.0 for the present formula, whereas it is 16.0 for the Bass model. Hence, the present model of the interaction barriers is also recommended for future applications for $59 \preceq z \preceq 313$ and the Bass model for $0 < z \preceq 59$.

The predictions of empirical model of the present work for fusion barrier height and interaction barrier height have been plotted in a new graph (figure 5) as a function of z to highlight the difference between the two, $B_{\rm int}$ and $B_{\rm fus}$. This figure reiterates clearly that for light nuclear systems these barriers are quite close, but for heavy nuclear systems ($z > 150$) they differ significantly. Obviously, $B_{\rm int}$ is smaller than $B_{\rm fu}$.

Table 10. Comparison of the interaction barrier B_{int} for different systems between the present empirical model, Bass interaction model [2] and available experimental values. The reactions are listed in the order of the increasing values of the z parameters. Mean squared errors for the Bass model and present formula are 15.22 and 1.74, respectively.

System	z	Bass	Pres.	Exptl.	System	z	Bass	Pres.	Exptl.
^{7}Li +^{64}Ni	14.21	8.31	4.12	12.2 [115]	^{12}C+^{205}Tl	59.37	56.29	55.59	56.0 [23]
^{6}Li +^{64}Ni	14.44	8.7	4.41	7.32 [116]	^{12}C+^{209}Bi	60.55	57.57	57.04	57.0 [23]
^{32}S+^{24}Mg	31.69	25.72	15.56		^{16}O+^{150}Nd	61.29	57.41	57.9	
^{32}S+^{27}Al	33.69	27.71	19.06		^{16}O+^{148}Nd	61.46	57.57	58.13	
^{18}O+^{64}Ni	33.83	28.37	19.31		^{12}C+^{238}U	65.04	62.63	62.38	62.2 [90]
^{6}Li+^{232}Th	33.91	29.51	27.51	30.3±0.06 [117]	^{35}Cl+^{64}Ni	65.46	60.18	62.87	
^{18}O+^{62}Ni	34.05	28.55	19.68		^{35}Cl+^{62}Ni	65.85	60.49	63.31	63.30 [54]
^{18}O+^{60}Ni	34.27	28.72	20.06		^{35}Cl+^{60}Ni	66.24	60.81	63.77	
^{16}O+^{64}Ni	34.36	28.85	20.2		^{35}Cl+^{58}Ni	66.65	61.13	64.24	64.2 [54]
^{18}O+^{58}Ni	34.51	28.91	20.45		^{14}N+^{238}U	74.82	72.83	73.47	73.4 [90]
^{16}O+^{62}Ni	34.58	29.03	20.58		^{16}O+^{205}Tl	76.99	74.6	75.85	77.0 [23]
^{16}O+^{60}Ni	34.81	29.21	20.97		^{16}O+^{238}U	84.43	82.92	83.84	82.5 [90]
^{18}O+^{65}Cu	34.93	29.47	21.17		^{30}Si+^{115}In	86.07	79.64	84.94	83 [118]
^{18}O+^{64}Cu	35.05	29.39	21.35		^{28}Si+^{115}In	86.84	80.42	85.75	83.15 [118]
^{18}O+^{63}Cu	35.15	29.64	21.54		^{35}Cl+^{90}Zr	87.71	83.57	87.29	
^{35}Cl+^{27}Al	35.24	29.28	21.69		^{40}Ar+^{110}Pd	100.84	98.01	100.77	
^{16}O+^{65}Cu	35.47	29.95	22.07		^{35}Cl+^{124}Sn	102.93	100.38	102.89	
^{18}O+^{70}Zn	35.59	30.21	22.28		^{20}Ne+^{238}U	103.24	102.81	103.19	102.0 [90]
^{16}O+^{63}Cu	35.69	30.13	22.44		^{28}Si +^{154}Sm	103.37	98.66	102.99	99.29 [119]
^{18}O+^{68}Zn	35.81	30.3	22.63		^{35}Cl+^{116}Sn	104.31	101.52	104.28	
^{18}O+^{66}Zn	36.02	30.55	22.98		^{40}Ar+^{164}Dy	133.57	133.93	133.37	135.0 [92]
^{16}O+^{70}Zn	36.14	30.71	23.17		^{40}Ar+^{197}Au	153.92	156.45	153.64	
^{18}O+^{64}Zn	36.25	30.73	23.35		^{40}Ar+^{208}Pb	157.95	161.08	157.69	
^{16}O+^{68}Zn	36.36	30.89	23.52		^{40}Ar+^{238}U	172.19	177.18	172.17	171.0 [3]
^{16}O+^{66}Zn	36.58	31.05	23.89		^{48}Ti+^{208}Pb	188.72	194.41	189.32	190.1 [13]
^{16}O+^{64}Zn	36.81	31.23	24.26		^{54}Cr+^{208}Pb	202.79	209.91	204.27	205.8 [13]
^{12}C+^{152}Sm	48.78	44.68	41.95		^{54}Cr+^{207}Pb	202.99	210.07	204.48	
^{18}O +^{124}Sn	52.58	45.99	48.71	49.3 [120]	^{52}Cr+^{208}Pb	203.78	210.79	205.34	
^{18}O +^{120}Sn	52.96	46.29	49.13	49.6 [120]	^{56}Fe+^{208}Pb	218.64	227.02	221.55	223.0 [13]
^{16}O +^{115}In	53.1	46.4	49.28	45.4 [118]	^{58}Ni+^{208}Pb	234.38	244.03	239.19	236.0 [13]
^{16}O +^{124}Sn	53.29	46.78	49.5	49.9 [120]	^{70}Zn+^{208}Pb	244.87	256.33	251.22	250.6 [13]
^{16}O +^{120}Sn	53.67	47.09	49.93	50.4 [120]	^{84}Kr+^{232}Th	307.86	326.78	328.62	332.0 [3]
^{35}Cl+^{48}Ti	54.16	48.39	49.06		^{84}Kr+^{238}U	313.14	332.81	––	333.0 [121]
^{16}O+^{134}Ba	58.66	54.44	54.72						

As discussed in the introduction, the motivation of the present work was to check the correct position of the observed resonance-like structures [16] with respect to the interaction or the fusion barrier. According to the Bass model [2,3], it is closer to the fusion barrier than the interaction barrier. It is thus opposite to the expectation. The scenario remains unchanged with the refined fusion and interaction barrier energies found in the present work for the systems ^{12}C(^{56}Fe, ^{56}Fe), ^{12}C(^{58}Ni, ^{58}Ni) and ^{12}C(^{63}Cu, ^{63}Cu). The physical reason for this anomaly is identified as a process called the nuclear orbiting resonance (dinuclear complexes) [73]. Details of this aspect are out of the scope of this work and will be published elsewhere.

7. Conclusion

In this paper, using the experimental values available in the literature, empirical formulae for the fusion and interaction barriers have been obtained. The experimental values available for the fusion barrier radius give us an option to find a formula for the fusion barrier radius also. The present study is restricted to the fusion and interaction barriers for the reactions in the regime $8 \leq z \leq 286$ and $59 \leq z \leq 313$, respectively. We have carried out a comparative study of the fusion barriers as well as the barrier radius between the present empirical formula and various empirical, semi-empirical models and microscopic theories along with the experimental results. After a thorough comparison with the experimental values, the present formula is found to be the best of all the models considered in this study for the said regions. Further, to examine its predictability, the fusion barrier and barrier radius have been used in the classic Wong fusion cross-section formula and the total fusion cross-sections are found to compare well with the experimental values. The fusion barrier and barrier radius obtained from the present formulae are used to solve the potential parameters of the Woods–Saxon potential using the three basic equations involved in eq. (3). The parameters so obtained are quite different from the ones used in the earlier studies.

The present fusion barrier formula is shown to be in excellent accordance with the experimental data in table 6. This comparison includes mostly the heavy-ion reactions aiming to synthesise the superheavy elements. Further, the agreement between the experimental and present interaction barrier formulae is pretty good. Hence, the present fusion and interaction barrier formulae together can be confidently used for planning experiments for the synthesis of the new superheavy elements. Similarly, current interaction barriers have been compared with the experimental interaction barriers quite well. We revealed in this work that the fusion and interaction barriers from the present work can be estimated very well and the predictions are better than the other models due to the wider experimental data considered. After all, it is an empirical formula. A refined and complete theoretical model such as DD-TDHF [63] is found to be even better than the present formula. More such theoretical calculations are highly desirable to shed better light on the reaction mechanism of the heavy-ion collisions. At the same time, a benchmark experiment that takes care of quasi-elastic events, deep inelastic collisions, capture reactions, etc. is of high demand for the heavy-ion reactions, in a proper manner.

Acknowledgements

The authors would like to acknowledge the illuminating discussions with Subir Nath, Ambar Chatterjee, B R Behra and S Kailas.

References

[1] B B Back, H Esbensen, C L Jiang and K E Rehm, *Rev. Mod. Phys.* **86(1)**, 317 (2014)
[2] R Bass, *Nucl. Phys. A* **231(1)**, 45 (1974)
[3] R Bass, Rainer, *Phys. Lett. B* **47(2)**, 139 (1973)
[4] B Blocki, J Randrup, W J Świątecki and C F Tsang, *Ann. Phys.* **105(2)**, 427 (1977)
[5] G R Satchler and W G Love, *Phys. Rep.* **55(3)**, 183 (1979)
[6] P R Christensen and A Winther, *Phys. Lett. B* **65(1)**, 19 (1976)
[7] W Reisdorf, *J. Phys. G* **20(9)**, 1297 (1994)
[8] A Winther, *Nucl. Phys. A* **594(2)**, 203 (1995)
[9] I Dutt and R K Puri, *Phys. Rev. C* **81(4)**, 044615 (2010)
[10] K Siwek-Wilczyńska and J Wilczyński, *Phys. Rev. C* **69(2)**, 024611 (2004)
[11] N Wang, W Xizhen, Z Li, M Liu and W Scheid, *Phys. Rev. C* **74(4)**, 044604 (2006)
[12] A S Freitas, L Marques, X X Zhang, M A Luzio, P Guillaumon, R P Condori and R Lichtenthäler, *Braz. J. Phys.* **46(1)**, 120 (2016).
[13] S Mitsuoka, H Ikezoe, K Nishio, K Tsuruta, S C Jeong, and Y Watanabe, *Phys. Rev. Lett.* **99(18)**, 182701 (2007)
[14] I Dutt and R K Puri, *Phys. Rev. C* **81(6)**, 064609 (2010)
[15] V I Zagrebaev, *Phys. Rev. C* **78(4)**, 047602 (2008)
[16] P Sharma and T Nandi, *Phys. Rev. Lett.* **119(20)**, 203401 (2017)
[17] T Banerjee, S Nath and S Pal, *Phys. Rev. C* **91(3)**, 034619 (2015)
[18] R Bass, *Phys. Rev. Lett.* **39(5)**, 265 (1977)

[19] N Rowley, G R Satchler and P H Stelson, *Phys. Lett. B* **254(1)**, 25 (1991)

[20] M V Andres, N Rowley and M A Nagarajun, *Phys. Lett. B* **202(3)**, 292 (1988)

[21] H Timmers, J R Leigh, M Dasgupta, D J Hinde, R C Lemmon, J C Mein, C R Morton, J O Newton and N Rowley, *Nucl. Phys. A* **584(1)**, 190 (1995)

[22] K Hagino and N Rowley, *Phys. Rev. C* **69(5)**, 054610 (2004)

[23] Y Le Beyec, M Lefort and M Sarda, *Nucl. Phys. A* **192(2)**, 405 (1972)

[24] J R Birkelund, L E Tubbs, J R Huizenga, J N De and D Sperber, *Phys. Rep.* **56(3)**, 107 (1979)

[25] W J Swikatecki, K Siwek-Wilczyńska, and J Wilczyński, *Phys. Rev. C* **71(1)**, 014602 (2005)

[26] H C Manjunatha, K N Sridhar, N Nagaraja and N Sowmya, *Eur. Phys. J. Plus* **133(6)**, 227 (2018)

[27] W D Myers and W J Swiatecki, *Phys. Rev. C* **62(4)**, 044610 (2000).

[28] P Möller, J R Nix, W D Myers and W J Swiatecki, *At. Data Nucl. Data Table* **59(2)**, 185 (1995)

[29] W D Myers and W J Swiatecki, *Ark. Fys.* **36(4)**, 343 (1967)

[30] M Liu, N Wang, Z Li, X Wu and E Zhao, *Nucl. Phys. A* **768(1)**, 80 (2006)

[31] J Bartel and K Bencheikh, *Eur. Phys. J. A* **14(2)**, 179 (2002)

[32] V Zanganeh, M Mirzaei and N Wang, *Commun. Theor. Phys.* **64(2)**, 177 (2015)

[33] R Moustabchir and G Royer, *Nucl. Phys. A* **683(1–4)**, 266 (2001)

[34] G Royer and B Remaud, *J. Phys. G* **10(8)**, 1057 (1984)

[35] G Giardina, F Hanappe, A I Muminov, A K Nasirov and L Stuttgè, *Nucl. Phys. A* **671(1–4)**, 165 (2000)

[36] N V Antonenko, E A Cherepanov, A K Nasirov, V P Permjakov and V V Volkov, *Phys. Lett. B* **319(4)**, 425 (1993)

[37] N V Antonenko, E A Cherepanov, A K Nasirov, V P Permjakov and V V Volkov, *Phys. Rev. C* **51(5)**, 2635 (1995)

[38] W Swiatecki, *Phys. Scr.* **24(1)**, 113 (1981)

[39] K Banerjee *et al*, *Phys. Rev. Lett.* **122(23)**, 232503 (2019)

[40] F Käppeler, F K Thielemann and M Wiescher, *Ann. Rev. Nucl. Part. Sci.* **48(1)**, 175 (1998)

[41] O K Ganiev and A K Nasirov, *J. Phys. G* **47(4)**, 045115 (2020)

[42] R Bass, *Nuclear reactions with heavy ion* (Springer, 1980)

[43] R A Broglia and A Winther, *Heavy ion reactions: The elementary processes* (Addison Wesley Publishing Company, 1991) Vol. 84

[44] A B Migdal, *Nucl. Phys.* **13(5)**, 655 (1959)

[45] G Bertsch, J Borysowicz, H McManus and W G Love, *Nucl. Phys. A* **284(3)**, 399 (1977)

[46] N Anantaraman, H Toki and G F Bertsch, *Nucl. Phys. A* **398(2)**, 269 (1983)

[47] H C Manjunatha, N Sowmya, N Manjunatha, P S Damodara Gupta, L Seenappa, K N Sridhar, T Ganesh and T Nandi, *Phys. Rev. C* **102(6)**, 064605 (2020)

[48] H C Manjunatha, L Seenappa, P S Damodara Gupta, N Manjunatha, K N Sridhar, N Sowmya and T Nandi, *Phys. Rev. C* **103(2)**, 024311 (2021)

[49] G Royer and R A Gherghescu, *Nucl. Phys. A* **699(3–4)**, 479 (2002)

[50] D N Poenaru and R A Gherghescu, *Phys. Rev. C* **94(1)**, 014309 (2016)

[51] G Royer, M Prince, X Scannell, I Lele-Cheudjou and A Samb, *Nucl. Phys. A* **1000**, 121811 (2020)

[52] H M Albers *et al*, *Phys. Lett. B* **808**, 135626 (2020)

[53] R O Akyuz and A Winther, *Proc. Enrico Fermi Int. School of Physics* **491** (1979)

[54] W Scobel, H H Gutbrod, M Blann and A Mignerey, *Phys. Rev. C* **14(5)**, 1808 (1976)

[55] M M Shaikh *et al*, *J. Phys. G* **45(9)**, 095103 (2018)

[56] J O Newton, R D Butt, M Dasgupta, D J Hinde, I I Gontchar, C R Morton and K Hagino, *Phys. Rev. C* **70(2)**, 024605 (2004)

[57] N Rowley, A Kabir and R Lindsay, *J. Phys. G* **15(12)**, L269 (1989)

[58] C Y Wong, *Phys. Rev. Lett.* **31(12)**, 766 (1973)

[59] K Hagino and N Takigawa, *Prog. Theor. Phys.* **128(6)**, 1061 (2012)

[60] R Gharaei and G L Zhang, *Nucl. Phys. A* **990**, 294 (2019)

[61] A M Stefanini *et al*, *Phys. Rev. C* **76(1)**, 014610 (2007)

[62] J W Negele, *Rev. Mod. Phys.* **54(4)**, 913 (1982)

[63] K Washiyama and D Lacroix, *Phys. Rev. C* **78(2)**, 024610 (2008)

[64] C Simenel, *Phys. Rev. Lett.* **105(19)**, 192701 (2010)

[65] C Simenel, R Keser, A S Umar and V E Oberacker, *Phys. Rev. C* **88(2)**, 024617 (2013)

[66] B Yilmaz, S Ayik, D Lacroix and K Washiyama, *Phys. Rev. C* **83(6)**, 064615 (2011)

[67] G Klotz-Engmann *et al*, *Nucl. Phys. A* **499(2)**, 392 (1989)

[68] W Swiatecki, *Prog. Part. Nucl. Phys.* **4**, 383 (1980)

[69] R Rafiei, R G Thomas, D J Hinde, M Dasgupta, C R Morton, L R Gasques, M L Brown, M D Rodriguez, *Phys. Rev. C* **77(2)**, 024606 (2008)

[70] A Diaz-Torres and I J Thompson, *Phys. Rev. C* **65(2)**, 024606 (2002).

[71] A Diaz-Torres, D J Hinde, J A Tostevin, M Dasgupta and L R Gasques, *Phys. Rev. Lett.* **98(15)**, 152701 (2007)

[72] R A Broglia, C H Dasso and A Winther, *Phys. Lett. B* **53(4)**, 301 (1974).

[73] P Braun-Munzinger, G M Berkowitz, T M Cormier, C M Jachcinski, J W and Harris, J Barrette and M J LeVine, *Phys. Rev. Lett.* **38(17)**, 944 (1977)

[74] L C Vaz, J M Alexander and G R Satchler, *Phys. Rep.* **69(5)**, 373 (1981).

[75] P Sperr, S Vigdor, Y Eisen, W Henning, D G Kovar, T R Ophel and B Zeidman, *Phys. Rev. Lett.* **36(8)**, 405 (1976)

[76] C M Jachcinski, D G Kovar, R R Betts, C N Davids, D F Geesaman, C Olmer, M Paul, S J Sanders and J L Yntema, *Phys. Rev. C* **24(5)**, 2070 (1981)
[77] Y Eisen, I Tserruya, Y Eyal, Y Fraenkel and M Hillman, *Nucl. Phys. A* **291(2)**, 459 (1977)
[78] S Gary and C Volant, *Phys. Rev. C* **25(4)**, 1877 (1982)
[79] G M Berkowitz, P Braun-Munzinger, J S Karp, R H Freifelder, T R Renner and H W Wilschut, *Phys. Rev. C* **28(2)**, 667 (1983)
[80] J O Newton, C R Morton, M Dasgupta, J R Leigh, J C Mein, D J Hinde, H Timmers and K Hagino, *Phys. Rev. C* **64(6)**, 064608 (2001)
[81] E F Aguilera, J J Kolata, P A DeYoung and J J Vega, *Phys. Rev. C* **33(6)**, 1961 (1986)
[82] H H Gutbrod, W G Winn and M Blann, *Phys. Rev. Lett.* **30(25)**, 1259 (1973)
[83] A Mukherjee, M Dasgupta, D J Hinde, K Hagino, J R Leigh, J C Mein, C R Morton, J O Newton and H Timmers, *Phys. Rev. C* **66(3)**, 034607 (2002)
[84] A M Stefanini *et al*, *Phys. Rev. C* **73(3)**, 034606 (2006)
[85] H Gauvin, Y Le Beyec and N T Porile, *Nucl. Phys. A* **223(1)**, 103 (1974)
[86] F Scarlassara, S Beghini, G Montagnoli, G F Segato, D Ackermann, L Corradi, C J Lin, A M Stefanini and L F Zheng, *Nucl. Phys. A* **672(1–4)**, 99 (2000)
[87] K Nishio, H Ikezoe, S Mitsuoka and J Lu, *Phys. Rev. C* **62(1)**, 014602 (2000)
[88] W Reisdorf *et al*, *Nucl. Phys. A* **438(1)**, 212 (1985)
[89] H Gauvin, Y Le Beyec, M Lefort and C Deprun, *Phys. Rev. Lett.* **28(11)**, 697 (1972)
[90] V E Viola Jr and T Sikkeland, *Phys. Rev.* **128(2)**, 767 (1962)
[91] D J Hinde, C R Morton, M Dasgupta, J R Leigh, J C Mein and H Timmers, *Nucl. Phys.* **592(2)**, 271 (1995)
[92] Y L Beyec, M Lefort and A Vigny, *Phys. Rev. C* **3(3)**, 1268 (1971)
[93] R Bimbot, H Gauvin, Y Le Beyec, M Lefort, N T Porile and B Tamain, *Nucl. Phys. A* **189(3)**, 539 (1972)
[94] M Lefort, C Ngo, J Peter and B Tamain, *Nucl. Phys. A* **216(1)**, 166 (1973)
[95] P Sperr, T H Braid, Y Eisen, D G Kovar, F W Prosser Jr, J P Schiffer, S L Tabor and S Vigdor, *Phys. Rev. Lett.* **37(6)**, 321 (1976).
[96] D Shapira, D DiGregorio, J G Del Campo, R A Dayras, J L C Ford Jr, A H Snell, P H Stelson, R G Stokstad and F Pougheon, *Phys. Rev. C* **28(3)**, 1148 (1983)
[97] P R S Gomes, T J P Penna, E F Chagas, R L Neto, J C Acquadro, P R Pascholati, E Crema, C Tenreiro, N Carlin Filho and M M Coimbra, *Nucl. Phys. A* **534(2)**, 429 (1991)
[98] L T Baby, V Tripathi, J J Das, P Sugathan, N Madhavan, A K Sinha, M C Radhakrishna, P V M Rao, S K Hui and K Hagino, *Phys. Rev. C* **62(1)**, 014603 (2000)
[99] A M Stefanini *et al*, *Nucl. Phys. A* **456(3)**, 509 (1986)
[100] A A Sonzogni, J D Bierman, M P Kelly, J P Lestone, J F Liang and R Vandenbosch, *Phys. Rev. C* **57(2)**, 722 (1998)
[101] J R Leigh *et al*, *Phys. Rev. C* **52(6)**, 3151 (1995)
[102] C R Morton, A C Berriman, M Dasgupta, D J Hinde, J O Newton, K Hagino and I J Thompson, *Phys. Rev. C* **60(4)**, 044608 (1999)
[103] A M Vinodkumar, K M Varier, N V S Prasad, D L Sastry, A K Sinha, N Madhavan, P Sugathan, D O Kataria and J J Das, *Phys. Rev. C* **53(2)**, 803 (1996)
[104] A M Stefanini, L Corradi, A M Vinodkumar, Y Feng, F Scarlassara, G Montagnoli, S Beghini and M Bisogno, *Phys. Rev. C* **62(1)**, 014601 (2000)
[105] H Timmers, D Ackermann, S Beghini, L Corradi, J H He, G Montagnoli, F Scarlassara, A M Stefanini and N Rowley, *Nucl. Phys. A* **633(3)**, 421 (1998)
[106] M Beckerman, M Salomaa, A Sperduto, H Enge, J Ball, A DiRienzo, S Gazes, Y Chen, J D Molitoris and M Nai-Feng, *Phys. Rev. Lett.* **45(18)**, 1472 (1980)
[107] M Beckerman, M Salomaa, A Sperduto, J D Molitoris and A DiRienzo, *Phys. Rev. C* **25(2)**, 837 (1982)
[108] S S Ntshangase *et al*, *Phys. Lett. B* **651(1)**, 27 (2007)
[109] M Trotta, A M Stefanini, L Corradi, A Gadea, F Scarlassara, S Beghini and G Montagnoli, *Phys. Rev. C* **65(1)**, 011601 (2001)
[110] M Klaassen, A Lindström, H Meltofte and T Piersma, *Nature* **413(6858)**, 794 (2001)
[111] D J Hinde, A C Berriman, M Dasgupta, J R Leigh, J C Mein, C R Morton and J O Newton, *Phys. Rev. C* **60(5)**, 054602 (1999)
[112] M Dasgupta, D J Hinde, J R Leigh, R C Lemmon, J C Mein, C R Morton, J O Newton and H Timmers, *Lectures on Probability and Second Order Random Fields* (1994)
[113] M Dasgupta, D J Hinde, N Rowley and A M Stefanini, *Ann. Rev. Nucl. Part. Sci.* **48(1)**, 401 (1998)
[114] J O Newton, R D Butt, M Dasgupta, D J Hinde, I I Gontchar, C R Morton and K Hagino, *Phys. Lett. B* **586(3–4)**, 219 (2004)
[115] M M Shaikh, S Roy, A Mukherjee, A Goswami, B Dey, S Pal, S Roy, A Shrivastava, S K Pandit and K Mahata, *Phys. Rev. C* **102(2)**, 024627 (2020)
[116] M M Shaikh, S Roy, S Rajbanshi, M K Pradhan, A Mukherjee, P Basu, S Pal, V Nanal, R G Pillay and A Shrivastava, *Phys. Rev. C* **91(3)**, 034615 (2015)
[117] S Mukherjee, B K Nayak, D S Monteiro, J Lubian, P R S Gomes, S Appannababu and R K Choudhury, *Phys. Rev. C* **80(1)**, 014607 (2009)
[118] B K Nayak, R K Choudhury, A Saxena, P K Sahu, R G Thomas, D C Biswas, B V John, E T Mirgule, Y K Gupta, M Bhike and H G Rajprakash, *Phys. Rev. C* **75(5)**, 054615 (2007)
[119] G Kaur, B R Behera, A Jhingan, B K Nayak, R Dubey, P Sharma, M Thakur, R Mahajan, N Saneesh, T Banerjee, Khushboo, A Kumar, S Mandal, A Saxena, P Sugathan and N Rowley, *Phys. Rev. C* **94(3)**, 034613 (2016)
[120] S Sinha, M R Pahlavani, R Varma, R K Choudhury, B K Nayak and A Saxena, *Phys. Rev. C* **64(2)**, 024607 (2001)
[121] L G Moretto, *Nucl. Phys. A* **180(2)**, 337 (1972)